Final Report

A Lyapunov Function Based Remedial Action Screening Tool Using Real-Time Data

March 2016

Prepared by

Prof. Joydeep Mitra
Dr. Mohammed Benidris
Nga Nguyen
Yuting Tian
Saleh Almasabi

FINAL REPORT

A LYAPUNOV FUNCTION BASED REMEDIAL ACTION SCREENING TOOL USING REAL-TIME DATA

A project funded by the U.S. Department of Energy, Award No. DE-OE0000625

Report Date: March 2016

Report Prepared by

Prof. Joydeep Mitra
Dr. Mohammed Benidris
Nga Nguyen
Yuting Tian
Saleh Almasabi

Project Contributors

Michigan State University (Project Lead)
- Prof. Joydeep Mitra (Principal Investigator)
- Dr. Mohammed Benidris
- Dr. Niannian Cai
- Nga Nguyen
- Yuting Tian
- Saleh Almasabi

Los Alamos National Laboratory
- Dr. Scott Backhaus
- Dr. Russell Bent
- Dr. Feng Pan
- Manuel Garcia

Southern California Edison
- Nagy Abed
- Farrokh Habibi-Ashrafi

Florida State University
- Prof. Omar Faruque
- Dr. Mischa Steurer
- Richard Meeker
- Michael Andrus
- Michael Sloderbeck
- Harsha Ravindra
- Md Kamrul Hasan Pulok
- Ali Hariri

LCG Consulting
- Dr. Rajat Deb
- Sidart Deb
- Dr. Benyamin Moradzadeh
- Andy Hoffman
- Basilio Bogado

EXECUTIVE SUMMARY

This report summarizes the outcome of a research project that comprised the development of a Lyapunov function based remedial action screening tool using real-time data (L-RAS). The L-RAS is an advanced computational tool that is intended to assist system operators in making real-time redispatch decisions to preserve power grid stability. The tool relies on screening contingencies using a homotopy method based on Lyapunov functions to avoid, to the extent possible, the use of time domain simulations. This enables transient stability evaluation at real-time speed without the use of massively parallel computational resources. The project combined the following components.

1. Development of a methodology for contingency screening using a homotopy method based on Lyapunov functions and real-time data.
2. Development of a methodology for recommending remedial actions based on the screening results.
3. Development of a visualization and operator interaction interface.
4. Testing of screening tool, validation of control actions, and demonstration of project outcomes on a representative real system simulated on a Real-Time Digital Simulator (RTDS) cluster.

The project was led by Michigan State University (MSU), where the theoretical models including homotopy-based screening, trajectory correction using real-time data, and remedial action were developed and implemented in the form of research-grade software. Los Alamos National Laboratory (LANL) contributed to the development of energy margin sensitivity dynamics, which constituted a part of the remedial action portfolio. Florida State University (FSU) and Southern California Edison (SCE) developed a model of the SCE system that was implemented on FSU's RTDS cluster to simulate real-time data that was streamed over the internet to MSU where the L-RAS tool was executed and remedial actions were communicated back to FSU to execute stabilizing controls on the simulated system. LCG Consulting developed the visualization and operator interaction interface, based on specifications provided by MSU.

The project was performed from October 2012 to December 2016, at the end of which the L-RAS tool, as described above, was completed and demonstrated. The project resulted in the following innovations and contributions: (a) the L-RAS software prototype, tested on a simulated system, vetted by utility personnel, and potentially ready for wider testing and commercialization; (b) an RTDS-based test bed that can be used for future research in the field; (c) a suite of breakthrough theoretical contributions to the field of power system stability and control; and (d) a new tool for visualization of power system stability margins.

While detailed descriptions of the development and implementation of the various project components have been provided in the quarterly reports, this final report provides an overview of the complete project, and is demonstrated using public domain test systems commonly used in the literature. The SCE system, and demonstrations thereon, are not included in this report due to Critical Energy Infrastructure Information (CEII) restrictions.

 This report was written with support of the U. S. Department of Energy under Contract No. DE-OE0000625.

ACKNOWLEDGMENTS

This research was funded by the U.S. Department of Energy, through the Office of Electricity Delivery & Energy Reliability, under the Advanced Modeling Grid Research Program Award No. DE-OE0000625. We thank Gilbert Bindewald III of the Office of Electricity and Raymond Lopez of the National Energy Technologies Laboratory for their continuous support and direction throughout the project.

TABLE OF CONTENTS

LIST OF TABLES

LIST OF FIGURES

1. Introduction

Modern power systems increasingly operate at lower security margins, due to reduced regulation capability resulting from increased variable generation and market operations. Consequently, they have grown increasingly vulnerable to cascading failures. Transient instability is a major contributing factor to cascading failures. The need for better situational awareness has also become evident, and triggered several ongoing efforts to develop improved methods of determining remedial action alternatives (including special protection schemes, emergency action, and on-line contingency analyses) and assist grid operators in making decisions. However, traditional contingency analyses have only evaluated static contingencies; dynamic contingencies were deemed too computationally intensive to solve in real-time. Stability scenarios were evaluated off-line, safe operating zones were determined and documented, and operators were required to be familiar with these scenarios and remedial actions. Recent technological advances have enabled these actions to be incorporated into SCADA (Supervisory Control and Data Acquisition) systems and EMS (Energy Management System), and these are now displayed in modern control rooms. Over the last few years, utilities and independent system operators (ISOs) have been working on integrating expert systems and screening tools into their control center practices.

The role of the Lyapunov function based remedial action screening tool using real-time data (L-RAS) can be understood thus. Following a potentially destabilizing event, the grid can evolve along any of numerous possible trajectories, which may be exacerbated by subsequent events or ameliorated by operator action. Using the tools available today, it is impossible to evaluate or screen every trajectory the system could assume; the computational challenge of performing time-domain simulation of every, or even a selected set of probable trajectories, within the time available to an operator, is simply unassailable. More recently, there have been theoretical advances that can potentially enable determination of security margins and perform remedial action screening in real-time. The L-RAS uses an approach based on Lyapunov functions to enable, without time-domain simulation, the selection of appropriate remedial actions that are most likely to result in stabilizing trajectories. If necessary, these trajectories may then be quickly evaluated using existing simulation tools. Now during the process of screening and evaluation of remedial actions, the system is still dynamically evolving, and it is necessary to update the tool using real-time data from the SCADA. This dynamic correction is an integral part of the L-RAS.

Upon identification of critical contingencies, remedial actions also require to be executed that can check the propagation of the disturbance and mitigate or even eliminate system disruption. These remedial actions are divided into preventive and corrective actions depending on system status and they include one or a combination of the following: generation rescheduling/tripping, load shedding, line tripping, voltage control, and utilization of FACTS

(Flexible AC Transmission Systems) devices. This project therefore combined emergent methods in real-time transient stability and remedial action screening (based on direct methods) with developments in telemetry and communication technologies to improve system security.

The objectives of the project were as follows.

1. To develop an energy function based method of transient stability analysis that can be solved at real-time speed without the use of massively parallel computation resources. The energy function is used for assessing global stability as well as local stability along with the determination of basin of attraction of the equilibrium solutions. The equilibrium solution of the power system dynamical model was determined using robust multi-parameter homotopy method.

2. To apply the method developed in (1) to perform remedial action screening at real-time speed. Also, develop research-grade algorithm implementing this feature.

3. To validate the methods and algorithms, including real-time performance, developed in (1) and (2), on a large-scale real-time digital simulator (RTDS). For this purpose, we used the 14-rack RTDS facility at the Florida State University Center for Advanced Power Systems (FSU-CAPS); this facility is capable of emulating a three-phase power system with up to 286 buses. We used data from Southern California Edison (SCE) to build a suitable reduced-order model. However, due to Critical Energy Infrastructure Information (CEII) restrictions, neither the SCE system, nor demonstrations thereon, are reported here. Instead, public domain test systems commonly used in the literature have been used here for purposed of illustration.

4. To incorporate in the tool described in (2) above the capability to update system status in real time. In order to achieve this, we acquire, at the project sites in Michigan State University (MSU), streaming data from FSU-CAPS, over the internet, to emulate telemetered data. We used in-house research-grade state estimation programs to generate system state information for the purpose of updating the screening tool.

5. To develop a visualization tool for operator interface. This tool incorporates basic functionality necessary to enable proof of concept demonstration of the tool possessing the features listed in (1), (2) and (4) above. The tool was developed by LCG Consulting (LCG).

Role of Lyapunov Methods and Real-time Data in Contingency Screening

In the past, transient stability contingency studies were limited to the system design or upgrade phase to yield stable and disturbance-rejecting power network design, and to operator training exercises in order to help with robust power system operations [1–4]. Up until now, complexities and computation overhead of computation associated with time domain analysis of transient stability problems have kept them from being run in real time to support decision-making in the event of and at the time of a disturbance. If a transient stability program could run in real-time or faster-than-real-time then power system control-room operators could be provided with a detailed view of the scope of cascading failures. Such a

view of the unfolding situation can assist an operator in comprehending the gravity of the emergent problem and its ramifications so that proactive counter-measures can be executed to limit the extent of the incident.

More recently, there have been theoretical advances that can potentially enable determination of security margins and perform remedial action screening in real-time. These methods are predominantly based on "direct" methods, such as Lyapunov or energy function methods. They utilize the advantages of the conservativeness of the direct methods to recursively classify the designated set of contingencies into *stable*, *potentially unstable* and *undetermined* subsets. The potentially unstable subset is further divided into stable, potentially unstable and undetermined subsets along the solution trajectory towards the controlling unstable equilibrium points (controlling UEPs). After using direct methods to screen out a large number of stable contingencies, time-domain simulations are performed to check those potentially unstable contingencies. Direct methods have proved to be very effective in reducing the number of contingencies that need further evaluation using time-domain simulations, and thereby made it possible to screen and compute dynamic contingencies in real-time. Thus, one saves significant computation time without compromising accuracy. If the initial condition does not belong to any basin of attraction or belongs to the basin of attraction of an unstable solution or belongs to the basin of attraction of an unrealizable equilibrium (e.g. solution in complex domain) then, time domain simulation is required to gather system trajectory. However, even under such a circumstance it is noted that, the initial condition search space, which is a subset of all the search space, may be significantly reduced. Further, if the evolving system state moves into one of the attractors for an equilibrium solution, then, further time-domain projection of dynamical path is not required for reasons explained above. Hence, the volume of time-domain simulation may not be significant, thereby saving the computational overhead and need for concurrent processing.

This project developed a real-time transient stability screening, remedial action and visualization tool. In combination with developments in telemetry and communication technologies, a visual interactive real-time transient stability screening and remedial action tool is developed to help the operators to improve the security and resilience of modern power systems. In developing the proposed real-time transient stability and remedial action screening tool, several technical challenges had to be solved including: (1) using the tools available today such as time-domain simulation, it is impossible to evaluate or screen every trajectory the system could assume within the time available to an operator, (2) updating the solver with real-time data while a contingency is dynamically evolving, (3) precise determination of the post-fault stable equilibrium points (SEPs) and controlling UEPs, and (4) prevailing practices inundate the operator with data, with little guidance on appropriate choices. For the challenge (1), the problem was tackled using energy function based methods of transient stability analysis that can be solved at real-time speed (or faster than real-time) without the use of massively parallel computation resources. For the challenge (2), the current practice of using energy function based methods is to assume that system frequency is constant which is not correct in simulating fault-on trajectories. During the process of screening and evaluation of remedial actions, the system is still dynamically evolving, and it is necessary to update the tool using real-time data. We have developed a scheme that dynamically adapts the region of stability according to real-time data streaming using phasor measurement units (PMU). It should be stated at the outset that it was not the purpose of this project to

contribute to or develop state estimation theory. The estimation of power system states from telemetered data is a mature field, and there is ample R&D in progress on the matter of modifying existing methods to take advantage of PMU data. Basic state estimation software was developed in-house for the purpose of updating the trajectories with real-time date. For the challenge (3), the accuracy of energy function based methods strongly relies on the determination of the controlling UEP. However, the presence of fractal shapes of the convergence region of the controlling UEP is the main reason of failure of many numerical methods in finding the correct controlling UEP. To find the correct controlling UEP, the initial guess, in using Newton methods for example, has to be within a certain neighborhood of the desired solution. This requirement makes it difficult to find the best guess and computationally expensive. In this work, we introduced a new method to compute the controlling UEP using robust multi-parameter homotopy method to determine the equilibrium solution of the power system dynamical model [5]. The homotopy method, being globally convergent, was developed to overcome issues with the local convergence of Newton methods. In other words, homotopy methods are guaranteed to converge to a solution regardless of an initial starting point provided that there are no singularities, bifurcation points, or turning points in its path. In the cases where there are multiple equilibrium points, the homotopy method has the ability to find those solutions. However, as we describe later, we have developed a method for confirming that homotopy does find the correct controlling UEP. For challenge (4), we have developed a visualization tool that significantly advances the state of the art, incorporate online updates, and provide live visualization for the suggested remedial actions. The interactive visualization tool incorporates the screening and remedial action tool for operator interface and to update system status in real time.

The proposed remedial action scheme helps operators in control rooms to choose an action that is appropriate for the prevailing conditions. The proposed remedial action scheme can be combined with the other tools using multi-decision-making techniques to choose the "best" option that has a minimum risk and minimum cost. The remedial action scheme is run periodically as well as after every triggering event. From the results of the analyzer (Energy Function Model), the remedial action scheme produces a list of actions that can alleviate the violation if there is any. The remedial action scheme is intended to act as a preventive/corrective action control. The ability of distinguishing between these two actions depends upon the initial conditions of the system and the triggering events. In case there is no disturbance, the proposed remedial action scheme examines the designated contingencies for possible transient stability violations. In case of potential violation, the scheme lists possible generation rescheduling alternatives based on the sensitivity of every control parameter on the energy margin and the best action is chosen based on multi-decision-making techniques. However, in the corrective action mode, the scheme is designed to prevent the possibility of cascading failures. The corrective action basically constitutes remedial action after the occurrence of a contingency, and aims to reduce the likelihood of system exacerbation. Therefore, a careful selection of the proposed actions needs to be implemented in this scheme. Possible actions from the corrective action scheme are generation redispatch or tripping, load shedding, and insertion braking resistors.

2. Real-Time Transient Stability Analysis

Real-Time transient stability assessment (TSA) has become an important requirement for modern power systems. However, the main challenge in Real-Time TSA lies in the complexity of the computations and the high computational burden that becomes necessary in order to accurately evaluate contingencies for stability.

Several methods and strategies have been proposed for on-line TSA. On-line TSA differs from real-time TSA in terms of the frequency of updating system status. While on-line TSA usually updates system status in a time frame of several seconds to minutes, real-time TSA updates system status in a time frame of milliseconds to seconds. On-line TSA can be classified into artificial intelligence (AI) approaches [6–21] and direct methods [2, 4, 22–27]. Due to the open-access operation of power system networks, the off-line analyses may not be fully correlated to the on-line data and therefore results of the AI approaches may become invalid [2]. On the other hand, direct methods for transient stability screening tools suffer from conservativeness of the results. However, these tools identify and exclude a large number of non-severe contingencies and apply detailed simulations on the severe or undetermined contingencies to reach the requirements of on-line applications. An on-line screening tool based on three levels of filtering using direct methods has been proposed in [22, 23]. Each level has two time frames: inertial transient filters and post-inertial transient filters. The filters screen the contingencies along the solution trajectory towards the controlling UEP (controlling unstable equilibrium point). Another on-line dynamic contingency screening tool based on the BCU (Boundary of stability region based Controlling Unstable equilibrium point) method is proposed in [2]. This tool uses six classifiers to screen out a small number of critical contingencies for detailed simulations. Improvements to the screening tool of [2] have been proposed in [24]. In the improved screening tool, the authors added another level of classification which is the detection of the islanding mode and improvements in the six classifiers of [2] by tuning the screening thresholds. This report presents a screening tool that classifies a designated set of contingencies (C) to stable (C_s) and unstable (C_u) subsets using homotopy-based (continuation) methods in real-time. These methods take advantage of the conservativeness of the Lyapunov methods to divide the classification process into stages. These stages are based on the size of the energy margin along system trajectory which is updated in real-time using Phasor Measurement Units (PMUs).

Existing on-line transient stability analysis tools based on direct methods have introduced several system dependent thresholds to classify a set of contingencies to stable, unstable or undetermined subsets. The undetermined contingencies are the contingencies that have numerical convergence problems such as failure to calculate the controlling UEP. In order for

these thresholds not to fail in classifying the contingencies, off-line transient stability analyses are required. Also, for the unstable or undetermined contingencies, detailed time-domain simulations are performed. Therefore, setting up the thresholds needs off-line transient stability assessments and may require an excessive use of time-domain simulations.

Several criteria and requirements are suggested in the literature for any on-line transient stability screening candidate which can be used for real-time transient stability screening. In [2], five requirements were suggested for any on-line transient stability screening tool. These requirements are, reliability measure, efficiency measure, on-line computation, speed measure, and performance measure. The reliability measure is defined as the absolute capture of the unstable contingencies. Efficiency measure indicates the ratio between the detected stable contingencies to the actual number of stable contingencies. On-line computation measure can be expressed in terms of the amount of use of off-line computations. Speed measure is used to evaluate computation speed. Performance measure tests robustness of the screening tools against the changes in operating conditions. The reliability, efficiency, and performance measures are related to the screening tool itself. On the other hand, on-line computation and speed measure are comparable indices that can be used to compare between alternative methods.

2.1 Direct Methods for Transient Stability Analysis

Direct methods have been successfully applied in evaluating the stability of power systems and deriving operating limits [1, 3, 28–32]. Given an n-generator system and assuming uniform damping, the classical model of the equations of motion of the generators with respect to the center of inertia (COI) can be denoted by [32]:

$$\dot{\tilde{\delta}}_i = \tilde{\omega}_i, \tag{2.1}$$

$$\dot{\tilde{\omega}}_i = \frac{1}{M_i}\left(P_{mi} - P_{ei}\right) - \frac{1}{M_T}P_{COI} - \lambda\tilde{\omega}_i, \tag{2.2}$$

$$\tilde{\delta}_i = \delta_i - \delta_o, \tag{2.3}$$

$$\tilde{\omega}_i = \omega_i - \omega_o, \tag{2.4}$$

$$\delta_o = \frac{1}{M_T}\sum_{i=1}^{n} M_i\delta_i, \tag{2.5}$$

$$\omega_o = \frac{1}{M_T}\sum_{i=1}^{n} M_i\omega_i, \tag{2.6}$$

$$M_T = \sum_{i=1}^{n} M_i, \tag{2.7}$$

where P_{mi} is the mechanical input of machine i, P_{ei} is the electrical power output of machine i, M_i is the inertia constant of machine i, δ_i is the power angle of machine i, ω_i is the angular

frequency of machine i, and λ is a uniform damping constant. The electrical power of machine i is given as follows.

$$P_{ei} = \sum_{j=1}^{n} E_i E_j \left[G_{ij} \cos\left(\tilde{\delta}_i - \tilde{\delta}_j\right) + B_{ij} \sin\left(\tilde{\delta}_i - \tilde{\delta}_j\right) \right], \tag{2.8}$$

where n is the number of machines in the system, E_i is the constant voltage magnitude, and G_{ij} and B_{ij} are the conductance and susceptance of the of the admittance matrix of the network-reduction model. The P_{COI} is computed as follows:

$$P_{COI} = \sum_{i=1}^{n} P_{mi} - \sum_{i=1}^{n} \sum_{j=1}^{n} E_i E_j \left[G_{ij} \cos\left(\tilde{\delta}_i - \tilde{\delta}_j\right) + B_{ij} \sin\left(\tilde{\delta}_i - \tilde{\delta}_j\right) \right], \tag{2.9}$$

The most commonly used energy function in transient stability analysis of power systems can be expressed as [28, 29]:

$$V = \frac{1}{2} \sum_{i=1}^{n} M_i \tilde{\omega}_i^2 - \sum_{i=1}^{n} P_i \left(\tilde{\delta}_i - \tilde{\delta}_i^s\right) - \sum_{i=1}^{n-1} \sum_{j=i+1}^{n} \left[C_{ij} \left(\cos\tilde{\delta}_{ij} - \cos\tilde{\delta}_{ij}^s \right) - I_{ij} \right], \tag{2.10}$$

where $P_i = P_{mi} - E_i^2 G_{ii}$, $C_{ij} = E_i E_j B_{ij}$, $\tilde{\delta}_{ij} = \tilde{\delta}_i - \tilde{\delta}_j$, the superscript s denotes the pre-fault stable equilibrium point, and I_{ij} is the energy dissipated in the network transfer conductances which can be expressed as follows.

$$I_{ij} = \int_{\tilde{\delta}_i^s + \tilde{\delta}_j^s}^{\tilde{\delta}_i + \tilde{\delta}_j} D_{ij} \cos\tilde{\delta}_{ij} \; d\left(\tilde{\delta}_i + \tilde{\delta}_j\right), \tag{2.11}$$

where $D_{ij} = E_i E_j G_{ij}$. This term is path dependent and can be calculated only if the system trajectory is known. Several methods are suggested in the literature to approximate this term. In this report, the method suggested in [28] is used which can be given as follows.

$$I_{ij} = D_{ij} \frac{\tilde{\delta}_i + \tilde{\delta}_j - \tilde{\delta}_i^s - \tilde{\delta}_j^s}{\tilde{\delta}_i - \tilde{\delta}_j - \tilde{\delta}_i^s + \tilde{\delta}_j^s} \left[\sin\tilde{\delta}_{ij} - \sin\tilde{\delta}_{ij}^s \right]. \tag{2.12}$$

Due to the approximation of the path dependent term in the energy function which accounts for transfer conductances, the accurate Exit Point (EP) may not be detected. The EP (see Fig. 2.1) is the point at which the projected fault-on trajectory exits the stability boundary of the post-fault stable equilibrium point (SEP). In the method presented in this report, an accurate EP is not necessary to find the controlling UEP.

2.2 Determination of the Controlling UEP

The Controlling UEP, using fault-on trajectory, is a UEP whose stable manifold, $W^s(X_{co})$, contains the EP of the fault-on trajectory as shown in Fig. 2.1.

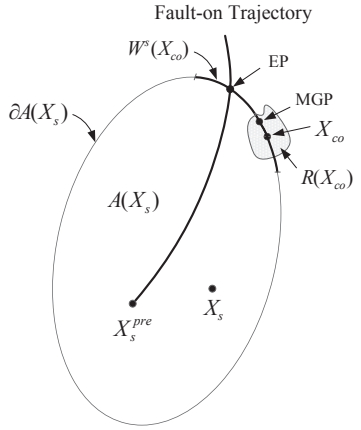

EP	is the exit point,
MGP	is the minimum gradient point,
X_{co}	is the controlling UEP,
$A(X_s)$	is the region of attraction (stability) of the post-fault stable equilibrium point (X_s),
$\partial A(X_s)$	is the boundary of the region of attraction,
$R(X_{co})$	is the region of convergence of the controlling UEP under Newton-Raphson method,
$W^s(X_{co})$	is the stable manifold of the controlling UEP,
X_s^{pre}	is the pre-fault stable equilibrium point.

Figure 2.1: Region of convergence of the controlling UEPs under the use of Newton-Raphson method. See [1] for details.

Computing the controlling UEP is crucial because the energy at a controlling UEP is used in computing the critical energy to assess the stability of the system. The dynamics of a power system, as given in (2.1) and (2.2), can be described in a compact form as a set of dynamic equations as follows.

$$\dot{x} = F(x). \tag{2.13}$$

A state vector x is called an equilibrium point x^* of the dynamic system represented in (2.13) if $F(x^*) = 0$. The controlling UEP is one of the unstable equilibrium points, but it is not an easy task to determine and distinguish it from the other unstable equilibrium points. A popular method to compute a controlling UEP is to use time-domain simulation of the projected fault-on trajectory to obtain the EP and minimum gradient point (MGP), and then use the MGP as an initial guess to find the controlling UEP by Newton-Raphson method. However, an inaccuracy in calculating the EP could cause a failure in calculating the MGP and then the controlling UEP. Most of the methods in the literature integrate the fault-on trajectory with large time step until the algorithm locates the EP between two time steps. The algorithm then bounds this point and starts searching for the EP using some tools, such as the golden section, linear and quadratic interpolation. Once a more accurate EP is discovered, the algorithm uses it as an initial point to compute the MGP and then the controlling UEP. Therefore, computing the controlling UEP is numerically involved and it requires significant effort to compute an accurate EP and MGP. In this report, two methods are used to calculate controlling UEPs, the BCU method and the homotopy-based method. In general, homotopy-based approaches are used to eliminate the problems associated with the choice of appropriate initial starting points. This report shows that a controlling UEP can be obtained by using homotopy-based approaches with an approximate EP as an initial point.

2.2.1 Characterization of the Region of Convergence of the Controlling UEPs

The accuracy of direct methods strongly relies on the determination of the controlling UEP. The region of convergence of an equilibrium point can be defined as follows: starting from an initial guess inside the region of convergence, a numerical method succeeds in finding the solution, or it fails if the initial guess lies outside this region. The size and shape of the region of convergence of a controlling UEP can be fractal and different for different numerical methods [1]. Therefore, the presence of fractal shapes of the convergence region of the controlling UEP is the main reason of failure of many numerical methods in finding the correct controlling UEP [1, 33, 34]. To find the correct controlling UEP, the initial guess, in using traditional iterative methods, has to be within a certain range of the desired solution. This requirement makes it difficult to find the best guess and renders the method computationally expensive.

In finding the correct controlling UEP, using other iterative methods, the EP, and the MGP have to be calculated first [35–41]. The controlling UEP, EP, and the MGP are shown in Fig. 2.1. Computationally, the EP is characterized by the first local maximum of the potential energy of the post-fault network along the projected fault-on trajectory. Another method to detect the EP is through detecting the change in the sign of the dot product of the post-fault power mismatch vector and the fault-on speed vector [1]. The MGP is numerically characterized by the first local minimum value of the norm of the vector field of the post-fault trajectory [1]. Most of the reported methods use the MGP as an initial point to generate a sequence of steps to find the controlling UEP. The robustness of finding the controlling UEP depends strongly on the accuracy of the calculation of MGP [36,37,39,41,42]. An inaccuracy in detecting the EP may cause difficulty in computing the MGP. However, detecting an accurate EP is computationally involved and sometimes it requires the use of interpolation methods after bounding the EP in a certain range. Therefore, a numerical inaccuracy in computing the EP might cause failure of numerical methods to calculate the controlling UEP.

2.2.2 Homotopy Method for Contingency Screening

Several methods have been proposed to compute the controlling UEP including the BCU method [35]. However, due to the problems associated with the detection of the EP and consequently the minimum gradient point, the BCU method occasionally encounters difficulty in finding a solution [39]. Despite the long history of applying direct methods in transient stability analysis, the problem of precise determination of the controlling UEP and the speed of computation are still of concern to many researchers.

One of the well-known methods in TSA using direct methods is the BCU method. The BCU method is a systematic method that uses the concept of reduced-state model for computing the controlling UEP [1,2]. This method defines an artificial model that can be solved to find all the equilibrium points of the original model. For each power system stability model there is a corresponding reduced-state model such that static and dynamic properties of the original model are captured to compute the controlling UEP on the stability boundary of the original model. Computing the controlling UEP using the BCU method on the

reduced-state model is easier than computing the controlling UEP of the original model [1]. For example, consider the following generic model [1]:

$$T\dot{x} = -\frac{\partial U}{\partial x}(x, y) + g_1(x, y), \tag{2.14}$$

$$\dot{y} = z, \tag{2.15}$$

$$M\dot{z} = -Dz - \frac{\partial U}{\partial y}(x, y) + g_2(x, y), \tag{2.16}$$

where x, y, and z are state variables, T is a positive definite matrix, M and D are diagonal positive definite matrices, U is the function of system dynamics, and $g_1(x, y)$ and $g_2(x, y)$ represent the transfer conductances.

The associated artificial, reduced-state model is given as follows [1]:

$$T\dot{x} = -\frac{\partial U}{\partial x}(x, y) + g_1(x, y), \tag{2.17}$$

$$\dot{y} = -\frac{\partial U}{\partial y}(x, y) + g_2(x, y). \tag{2.18}$$

The general procedure of finding the controlling UEP using the BCU method is summarized as follows [35]. The definitions are referred to Fig. 2.1.

1. From the fault-on trajectory, determine the EP.
2. Use the EP as an initial point and integrate the post-fault reduced-state model to find the MGP.
3. Use the MGP as an initial point to calculate the controlling UEP of the reduced-state model.
4. Determine the controlling UEP of the original system.

In implementing the above procedure, it is important to be aware of several potential numerical issues [1]. For example, an inaccuracy in calculating the EP may cause an inaccuracy in computing the MGP. If the computed MGP is not sufficiently close to the controlling UEP, the iterative method may diverge or converge to another equilibrium point. Two situations where the EP may not be accurate (either inside the stability region or outside the stability region) are shown in Fig. 2.2.

From Fig. 2.2, it can be seen that an inaccurate EP can lead to failure of calculating the controlling UEP [1]. A procedure that can be used to solve this problem is called stability-boundary-following procedure [2]. The procedure can be summarized as follows [2]: starting from the given EP, integrate the post-fault model for a few iterations (e.g., three to five iterations) and check if the MGP has been detected. If it has been detected, check if the controlling UEP can be computed using this MGP. If the MGP has not been detected or the controlling UEP cannot be computed (either converges to the post-fault SEP or the distance between the computed controlling UEP and the MGP is larger than a threshold), draw a ray connecting the current point on the post-fault trajectory with the post-fault SEP and search along this trajectory for a new MGP. This procedure is depicted in Fig. 2.3 for the case where the EP lies inside the stability region. Full description of this procedure is given in [2].

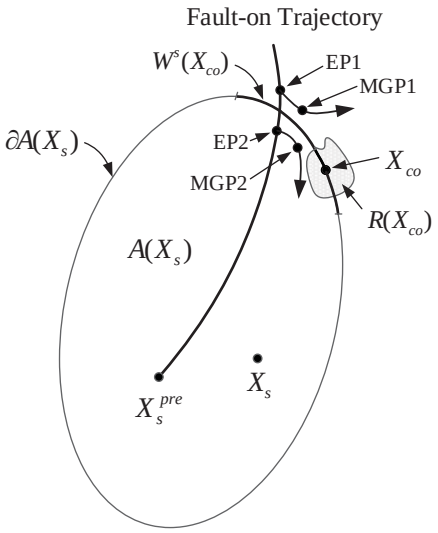

EP1 Exit point 1,
EP2 Exit point 2,
MGP1 Minimum gradient point corresponding to EP1,
MGP2 Minimum gradient point corresponding to EP2.

Figure 2.2: The effect of an inaccurate EP on the calculation of the MGP.

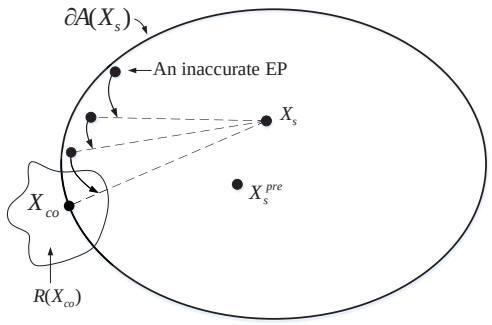

Figure 2.3: A stability-boundary-following procedure. See [2] for details.

Due to the difficulties associated with determining the controlling UEPs which in turn are attributed to numerical problems in calculating the EPs and MGPs, we have applied a homotopy based method to calculate the controlling UEPs [43]. We have found that the proposed homotopy based method is robust, reliable, and efficient in calculating the controlling UEP. Also, homotopy methods are not sensitive to the initial points.

While homotopy-based approaches are known to be reliable in finding a solution, they are intrinsically slow because these methods map the trajectory of the solution from an easy and known solution to the desired solution. In this project we developed an algorithm that uses homotopy-based approaches with EPs as the initial points to find controlling UEPs. Using approximate EPs rather than computing accurate EPs, as is common practice in finding the controlling UEP, the intrinsic slow speed of computation of homotopy-based approaches is compensated. Further, homotopy-based approaches eliminate the necessity of computing the MGP, which makes the homotopy-based approach comparable with iterative methods in terms of the speed of computation.

Homotopy-based approaches have been successfully applied in computing the closest

UEP but not the controlling UEP [44, 45]. The closest UEP can be distinguished by having the lowest energy function value. The approaches reported in these references utilize the strategy of singular fixed-point and the concept of bifurcation to locate the closest UEP. The algorithm proceeds by choosing a set of initial points that, by using homotopy-based approaches, converge to a set of type-1 UEPs (a UEP that has one unstable eigenvalue in the Jacobian matrix). By choosing a set of proper initial points, the resulting set of the type-1 UEPs includes the closest UEP. Chen *et al.* in [37] have used the continuation-based methods without the use of the energy function and approximating the stability boundary locally.

Homotopy is a numerical method to solve and find the roots of non-linear systems expressed as $F(x) = 0$. It is also called continuous Newton-Raphson method. Homotopy is known to be a reliable method to find solutions and it is not sensitive to the initial conditions as compared with the other iterative methods. However, when multiple solutions exist, a better initial condition helps obtain the solution of interest first. In applying homotopy-based methods, the pre-fault SEP is used as an initial and known solution to calculate the post-fault SEP and the EP is used as an initial and known solution to calculate the controlling UEP.

Computing an accurate EP is not an easy task and computing the MGP depends on the accuracy of the EP. In applying homotopy-based approaches to calculate the controlling UEP, a less accurate EP as a known solution can be used. The justification is that with an EP as the initial guess, homotopy-based approaches can find the controlling UEP first since its location is the closest to the EP in terms of the energy value.

The basic idea of the homotopy method is to find the solutions by path continuation, starting at a known solution x^0 that satisfies $G(x^0) = 0$. The homotopy method traces the solution trajectory by a predictor-corrector algorithm to get a solution of the original equation. The most widely used homotopy function is expressed as follows.

$$H(x,t) = tF(x) + (1-t)G(x) = 0, \tag{2.19}$$

where t changes from 0 to 1 with an incremental step-size through the mapping process, i.e., $H(x,0) = G(x)$ and $H(x,1) = F(x)$.

The function $G(x)$ can be chosen arbitrarily as long as it has a known solution. The Newton-homotopy can be expressed as follows.

$$G(x) = F(x) - F(x^0), \tag{2.20}$$

where x^0 can be any starting point. Therefore, the homotopy function becomes

$$H(x,t) = F(x) - (1-t)F(x^0) = 0. \tag{2.21}$$

Direction of Solution Mapping

It should be noted that in applying homotopy methods, the direction of the search (forward or backward) for the solution is an important factor in determining the correct controlling UEPs. In backward direction, the mapping factor is considered negative. Therefore, equation (2.19) can be expressed as follows.

$$H(x,t) = tF(x) + (1+t)G(x) = 0. \tag{2.22}$$

The direction of the search depends on the location of the exit point with respect to the controlling UEP on the stability boundary. If this direction is unknown and if the forward direction (for example) is performed, the solution trajectory may converge to an unstable equilibrium point (UEP) but not the controlling UEP. Fig. 2.4 shows a case where the controlling UEP is located in the direction of forward mapping from the exit point. If the backward mapping were used, the solution trajectory would converge to another UEP but not the controlling UEP. Also, Fig. 2.5 shows a case where the controlling UEP is located in the direction of backward mapping from the exit point. If the forward mapping were used, the solution trajectory would converge to a different UEP. During the calculation process, the algorithm proceeds by assuming forward mapping for one homotopy iteration; if the solution diverges or converges to a point far from the exit point, the algorithm uses backward mapping.

The speed of calculation depends on the closeness of the initial points to the the controlling UEP. For the studied systems, the number of the homotopy iterations to arrive to the controlling UEP starting from the exit point ranges from one to three iterations where each homotopy iteration is equivalent to a full Newton (or other method) solution. This can be justified by the fact that if the initial point is at or close to the MGP, the algorithm takes one iteration which is equivalent to the BCU method. However, if the initial point is the exit point, the proposed method takes two or more iterations.

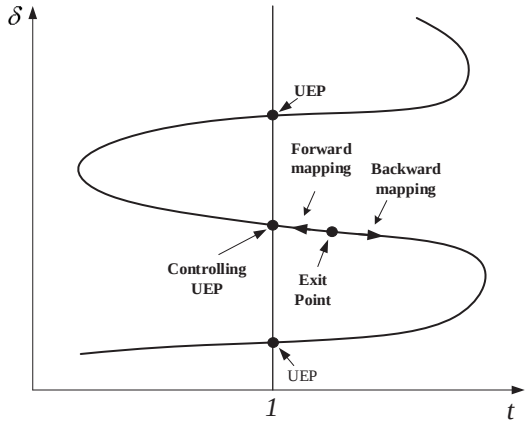

Figure 2.4: Forward and Backward search for the controlling UEP - the backward mapping converges to a UEP not the controlling UEP.

Example

To demonstrate the application of the proposed homotopy-based approach in computing controlling UEPs using exit points as initial points, we have applied this method on several systems including the Southern California Edison system, the equivalent WECC (Western Electricity Coordinating Council) system and the New England 39 bus system. In this example, we present the results for the WECC system. System configuration is shown in Fig. 2.6. Intel Fortran is used to generate an executable file that calculates the exit points

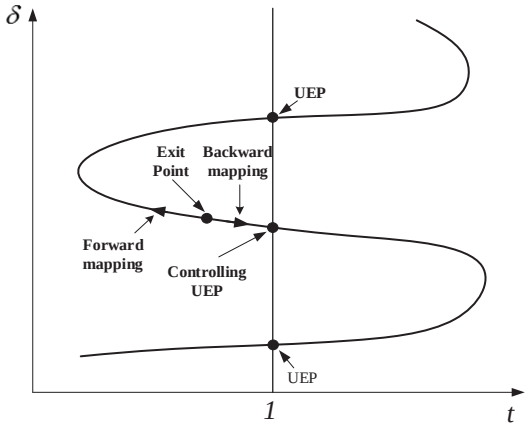

Figure 2.5: Forward and Backward search for the controlling UEP - the forward mapping converges to a UEP not the controlling UEP.

and then the controlling UEPs. The program has succeeded to find all the exit points and controlling UEPs.

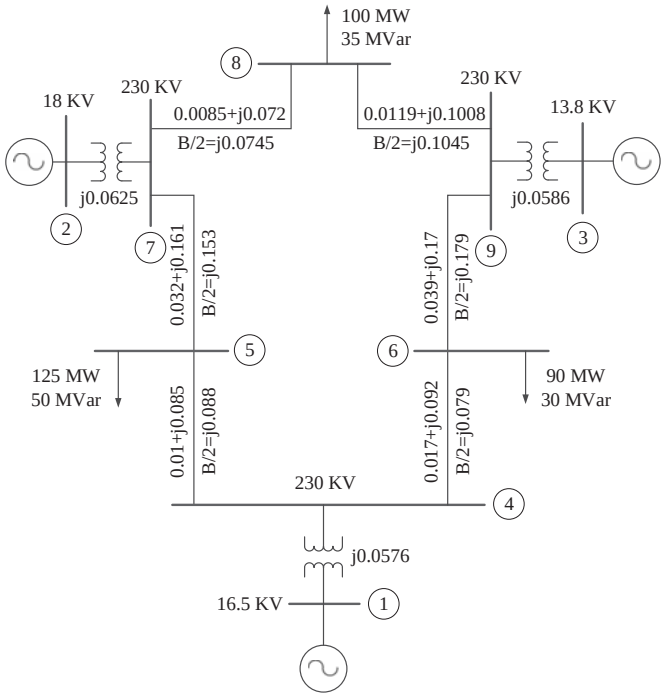

Figure 2.6: WECC system configuration.

Ther WECC Test System consists of 3 generators, 9 buses and six transmission lines [1]. The exit points associated with the designated 12 contingencies are shown in Table 2.1.

The exit points are used as initial conditions to calculate the controlling UEPs. To show the solution trajectories of the Newton-homotopy method for these contingencies, we have

Table 2.1: Contingency list details and the corresponding exit points.

No.	Fault at Bus	Line Trip From	Line Trip To	Exit points, (rad) $\tilde{\delta}_1$	$\tilde{\delta}_2$	$\tilde{\delta}_3$
1	4	4	5	−0.83157	2.05223	2.16748
2	5	4	5	−0.85604	2.24468	1.95048
3	4	4	6	−0.82573	2.00656	2.22575
4	6	4	6	−0.82663	2.00656	2.22575
5	5	5	7	−0.77351	2.07331	1.66662
6	7	5	7	−0.84828	2.68764	0.94769
7	6	6	9	−0.75797	1.83370	2.05405
8	9	6	9	−0.50293	0.51129	2.86278
9	7	7	8	−0.73581	2.28572	0.91888
10	8	7	8	−0.77159	1.74633	2.34681
11	8	8	9	−0.76930	1.74136	2.33940
12	9	8	9	−0.45872	0.48828	2.56452

selected generator #1 to be a reference for plotting purposes only in order for the trajectories to appear in three-dimension plots. That is, generator #1 was taken as a reference for the plotting only and the calculations were carried out using the COI as a reference frame. Fig. 2.7, Fig. 2.8 and Fig. 2.9 show the trajectories of the solutions for the first three contingencies where CUEP denotes the controlling UEP. The trajectories show the solution process starting from the exit points to the controlling UEPs while changing the homotopy factor t.

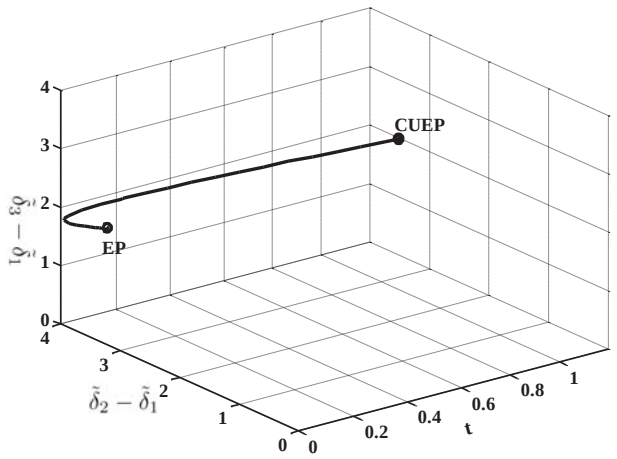

Figure 2.7: Solution trajectory using Newton-homotopy—Contingency #1.

The controlling UEPs of the 12 designated contingencies are shown in Table 2.2. Starting from the exit points of Table 2.1, the algorithm converged to these controlling UEPs.

To test the performance of the proposed approach, less accurate exit points (by utilizing large step size in calculating the exit points), have been used in calculating the controlling UEPs. Less accurate exit points are easy to calculate but they are expected to cause numeri-

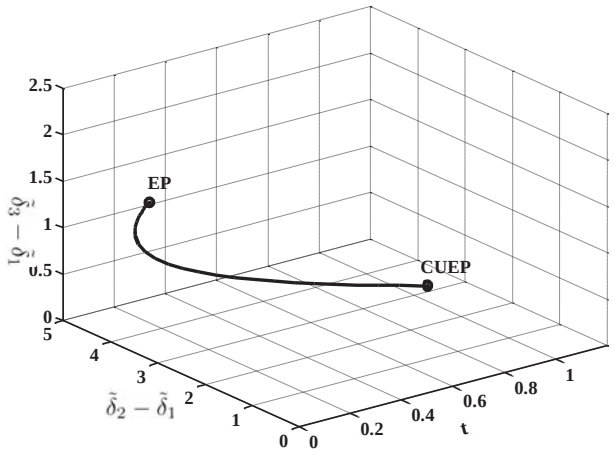

Figure 2.8: Solution trajectory using Newton-homotopy—Contingency #2.

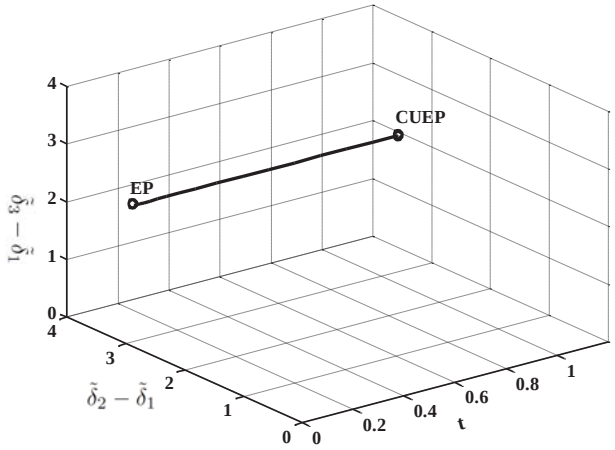

Figure 2.9: Solution trajectory using Newton-homotopy—Contingency #3.

cal problems when attempting to use conventional iterative methods. The homotopy-based approach has succeeded in calculating all the controlling UEPs providing that the exit points are not very accurate.

2.3 Filtering Using Homotopy Method

Screening and classification processes require sophisticated programs that can meet the requirements of on-line applications. The existing on-line transient stability analysis tools based on transient stability direct methods have introduced several system dependent thresholds for classifications. These thresholds are used to classify a set of contingencies into stable, unstable or undetermined subsets. The undetermined contingencies are the contingencies that have numerical convergence problems such as failure to calculate the controlling unstable equilibrium point, controlling UEP. In order for these thresholds not to fail in classifying the contingencies, off-line transient stability analyses are required. Also, for the unstable or undetermined contingencies, detailed time-domain simulations are performed. Therefore, these

Table 2.2: The computed controlling UEPs using homotopy method.

No.	Fault near Bus	Line Trip From	Line Trip To	Controlling UEPs, (rad) $\tilde{\delta}_1$	$\tilde{\delta}_2$	$\tilde{\delta}_3$
1	4	4	5	−0.8323	2.0742	2.1447
2	5	4	5	−0.8323	2.0742	2.1447
3	4	4	6	−0.8266	2.0821	2.0540
4	6	4	6	−0.8266	2.0821	2.0540
5	5	5	7	−0.7598	1.9521	1.8071
6	7	5	7	−0.7598	1.9521	1.8071
7	6	6	9	−0.7586	1.8576	1.9979
8	9	6	9	−0.7586	1.8576	1.9979
9	7	7	8	−0.5430	2.1797	−0.3764
10	8	7	8	−0.3500	0.0738	2.5861
11	8	8	9	−0.2915	−0.1017	2.5004
12	9	8	9	−0.2915	−0.1017	2.5004

methods require off-line transient stability assessments and may excessively use time-domain simulations.

Several criteria and requirements are suggested in the literature for any on-line transient stability screening candidate. In [2], five requirements were suggested for any on-line transient stability screening tool. These requirements are, reliability measure, efficiency measure, on-line computation, speed measure and performance measure [2]. The reliability measure is defined as the absolute capture of the unstable contingencies. Efficiency measure indicates the ratio between the detected stable contingencies to the actual number of stable contingencies. On-line computation measure can be defined as little need of off-line computations. Speed measure is used to evaluate computation speed. Performance measure tests robustness of the proposed tool against the changes in operating conditions. The reliability, efficiency and performance measures are related to the screening tool itself. On the other hand, on-line computation and speed measure are comparable indices that can be used to compare between two alternatives for example.

The proposed transient stability screening tool checks stability by sequentially calculating exit point, minimum gradient point and controlling UEP for each contingency. In this stage of developing the proposed screening tool, the tool is not intended to check the stability of the contingencies at the exit points or at the minimum gradient points as most of the current contingency screening tools do. In this stage, the work is intended to test the screening procedures with the introduction of the use of the homotopy-based approaches. Several methods can be used to increase the speed of computation such as using some indicators and thresholds to drop off, at the early stages of screening, mild contingencies, i.e. highly stable contingencies.

Homotopy-based approach is adopted in the proposed screening tool to calculate the desired solution if the iterative methods such as Newton method fails to converge to the desired solution. In transient stability screening of large systems, numerical problems in calculating pre-fault SEPs, exit points, MGPs and controlling UEPs are expected to be encountered. In

the exiting transient stability screening tools using direct methods, if the iterative methods fail to converge to the desired solution, time-domain simulations are performed to check the stability. Therefore, if the number of contingencies that have numerical problems is very large, an excessive use of time-domain simulations is required and the screening tool may not meet the requirements of on-line applications.

Some indicators to test the convergence of the solution are adapted from [2]. Two indicators are used in detecting the convergence problems in calculating the post-fault SEP. These indicators are the maximum number of iterations which was assumed to be 5 iterations and the maximum angle difference between the pre-fault SEP and post-fault SEP which was assumed to be 30°. Also, two indicators are used in detecting a numerical convergence problem in calculating the controlling UEP which are the maximum number of iterations and the maximum angle difference between the MGP and the computed controlling UEP. The maximum number of iterations was assumed 10 iterations and the maximum angle difference was assumed 120°.

2.4 Transient Stability Screening Procedure

The concept of transient stability filtering of section 2.3 is depicted in Fig. 2.10. The inputs of the screening tool are taken from the system state estimator and a designated set of contingencies. From the output of the screening tool, the unstable contingencies are sent the to remedial action tool. This work deals with the screening tool itself and the on-line data, state estimator and remedial action tool are out of the scope of this project. The screening procedures start with calculating the post-fault SEP for each contingency using Newton method. If the Newton method succeeds in finding the post-fault SEP, the program continues to calculate the exit point. On the other hand, if Newton method fails to find the post-fault SEP, the program activates the homotopy-based approach using the pre-fault SEP as initial and known solution. If the homotopy-based approach succeeds to find the solution, the program proceeds to calculate the exit point and if it fails, the program sends the contingency to the time-domain simulator.

If the exit point has been found, the program proceeds to calculate the MGP; otherwise it sends the contingency to the time-domain simulator. The program sends the contingency to the time-domain simulator because without knowing the exit point, neither the iterative methods nor the homotopy-based methods can converge to the controlling UEP. If the MGP has been calculated successfully, the program continues to calculate the controlling UEP. If the MGP has not been found or the iterative method fails to calculate the controlling UEP using the MGP as an initial condition, the program activates the homotopy-based approach to calculate the controlling UEP using the exit point as initial and known solution. If the algorithm succeeds to calculate the controlling UEP either using the Newton method or the homotopy-based approach, the program uses the energy margin as an criterion for classifying the contingency either as stable or as unstable. If the homotopy-based approach fails to calculate the controlling UEP, time-domain simulation has to be performed. The stable and unstable contingencies are classified into two subsets. If all the contingencies in the list are scanned, the program outputs the results; otherwise it continues to the next contingency.

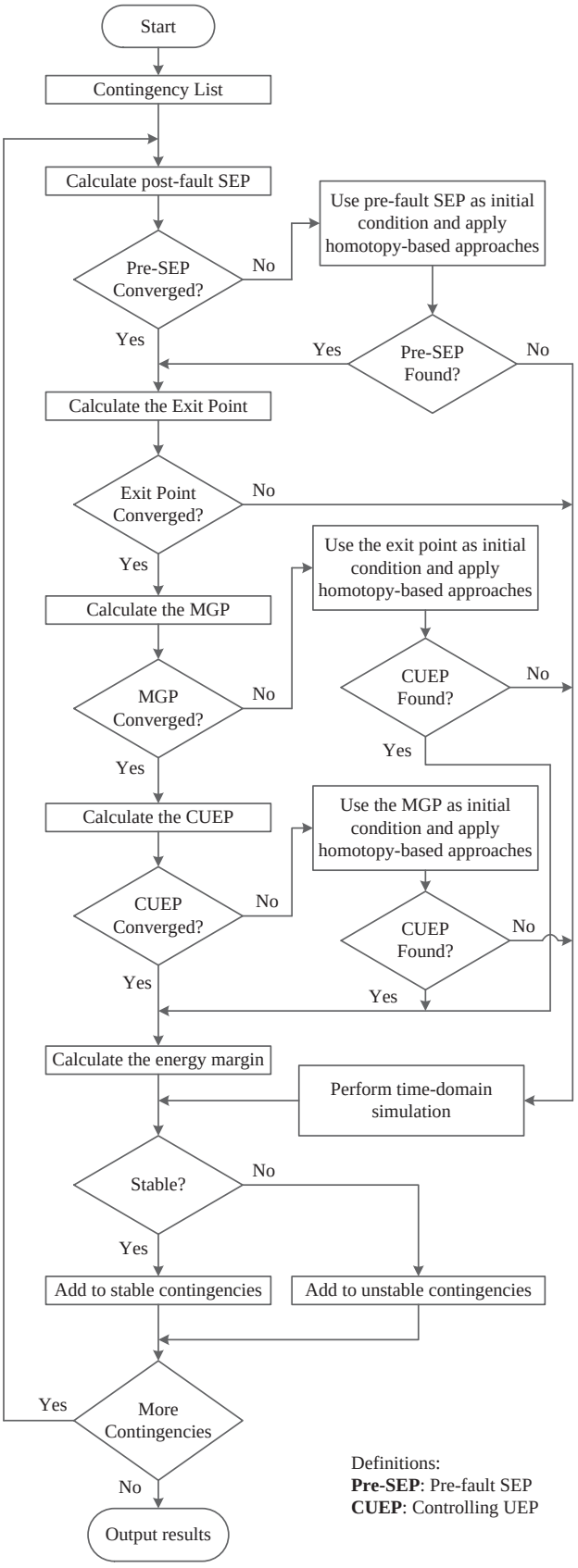

Figure 2.10: Flowchart of the screening tool.

3. Remedial Actions

There are two types of remedial actions, namely, corrective actions and preventive actions. Corrective actions can be performed locally or globally depending on the available measurements and means. On the other hand, preventive actions are performed globally. Global corrective actions could be generation tripping, load shedding, line tripping and local corrective actions could be control of excitation and output power. The preventive actions could be generation rescheduling and load shedding. The ability to distinguish between these actions depends upon the initial conditions of the system and the triggering events. For example, in a case where there is no disturbance, the remedial action scheme examines the designated contingencies for possible transient stability violations. In case of a possible violation, the scheme lists possible generation rescheduling alternatives based on the sensitivity of every control parameter on the energy margin. However, in case of corrective action mode, the scheme is designed to prevent the possibility of cascading failures. The corrective action scheme is less costly than the preventive action; however, it is the last line of defense and if the correction actions suggested by this scheme cannot be applied, the system is more likely to undergo cascading failures. Therefore, a careful selection of the actions needs to be implemented in this scheme.

After screening, contingencies are divided into two main groups: stable and unstable. With the stable group, no control actions are needed to intervene in system operation. However, with unstable contingencies, control measures are required to prevent unacceptable impact on system stability (preventive actions) or to immediately respond to the occurring disturbance in order to maintain system operation in balance (corrective action).

The philosophy of distinguishing between the corrective and preventive remedial actions is explained as follows. The preventive screening and the suggested remedial actions can be triggered either periodically or upon operator request. The preventive action tool starts with screening a full list of possible contingencies assuming the system resides in a healthy state. On the other hand, the corrective screening and the suggested remedial actions are triggered immediately after an occurrence of an event. Here, instead of screening the entire set of possible contingencies, only the "related" contingencies and the possible contingencies on some critical lines are screened. When a fault occurs at some location in the grid, the neighboring lines are exposed to overload and/or false tripping due to hidden failures in the protection equipments [46]. Also, some critical lines that carry a large amount of power, transient stability-limited lines, and the inter-ties between areas may be affected by faults in non-neighboring lines. The process of performing remedial action control is shown in Fig. 3.1.

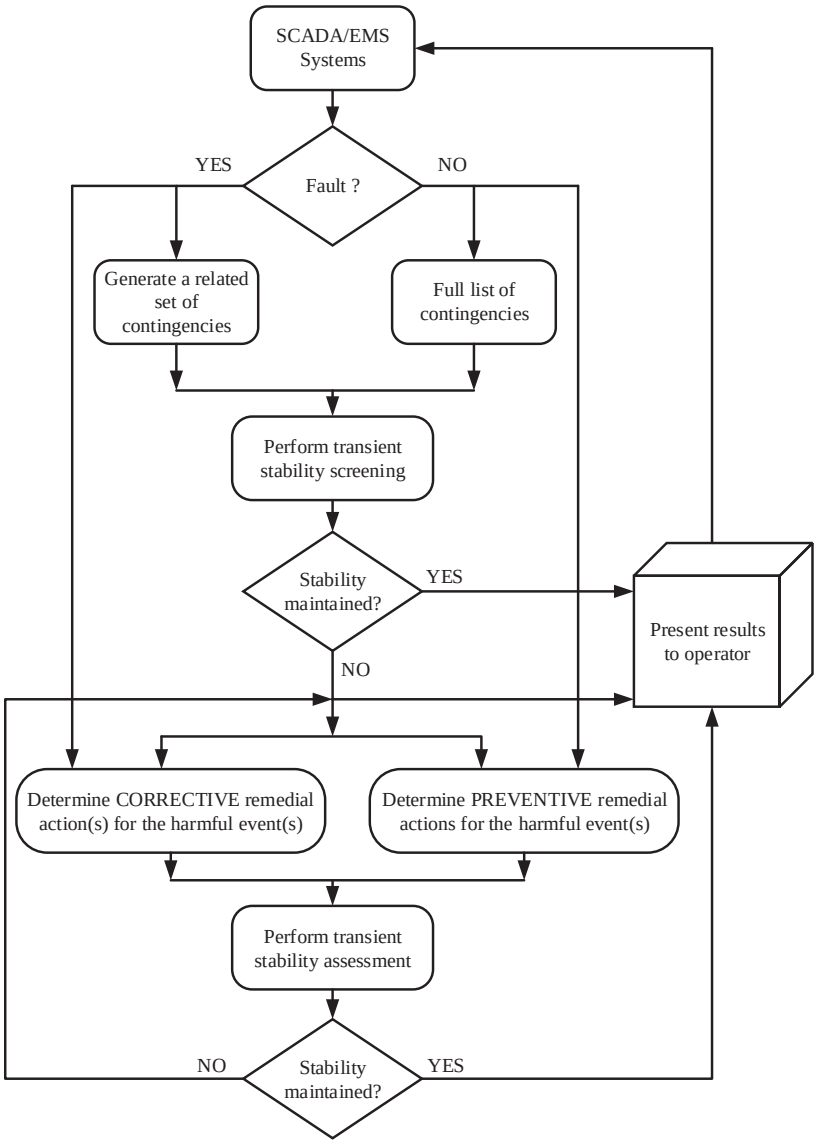

Figure 3.1: Flowchart of the corrective and preventive remedial actions scheme.

3.1 Energy Margin and Sensitivity Analysis-based Remedial Action Control

The energy margin (ΔV) is defined as the difference between the value of the energy function V at the instant of clearing, V^{cl}, and at the controlling UEP to determine the critical value V^{u} (the critical value of energy margin is calculated at the controlling UEP). This condition is mathematically expressed by the following equation [47]:

$$\Delta V = V^{u} - V^{cl}. \tag{3.1}$$

If the difference is larger than zero, the system is deemed stable; otherwise, it is deemed unstable. The energy margin is calculated as follows [47].

$$\begin{aligned}\Delta V = &-\frac{1}{2}M_{eq}(\tilde{\omega}_{eq}^{cl})^2 - \sum_{i=1}^{n} P_i(\tilde{\delta}_i^u - \tilde{\delta}_i^{cl}) - \sum_{i=1}^{n-1}\sum_{j=i+1}^{n}[C_{ij}(\cos\tilde{\delta}_{ij}^u - \cos\tilde{\delta}_{ij}^{cl}) \\ &- D_{ij}\frac{\tilde{\delta}_i^u + \tilde{\delta}_j^u - \tilde{\delta}_i^{cl} - \tilde{\delta}_j^{cl}}{\tilde{\delta}_{ij}^u - \tilde{\delta}_{ij}^{cl}}(\sin\tilde{\delta}_{ij}^u - \sin\tilde{\delta}_{ij}^{cl})] \\ &= \Delta V_{KE} + \Delta V_{PE},\end{aligned}$$

where $M_{eq} = \frac{M_{cr}M_{sys}}{M_{cr}+M_{sys}}$, $\widetilde{\omega}_{eq}^{cl} = \widetilde{\omega}_{cr}^{cl} - \widetilde{\omega}_{sys}^{cl}$, M_{cr} and M_{sys} are the total inertia of all machines with advanced rotor angle and total inertia of the rest of machines, respectively, at the calculated controlling UEP, $\tilde{\omega}_{cr}^{cl}$ and $\tilde{\omega}_{sys}^{cl}$ are the velocity of machines with advanced rotor angle and the rest of machines, respectively, referred to the COI reference frame at the clearing of the disturbance, ΔV_{KE} and ΔP_{PE} are the change in the kinetic energy and the potential energy, respectively.

3.1.1 Concept of Energy Margin Sensitivity

As can be seen from equation (3.2), the energy margin is a multi-variable function and can be expressed as:

$$\Delta V = f(P_m, \tilde{\delta}^u, \tilde{\delta}^{cl}, \dot{\tilde{\delta}}^{cl}, E, G_{ij}, B_{ij}). \tag{3.2}$$

When shifting the scheduled power among generators, the changes in clearing speeds, clearing angles, controlling UEP and the voltages behind E_i are considerable. The changes in G_{ij} and B_{ij} are neglected because of their small values. Due to the small size of generation changes, it is assumed that the high order terms in the sensitivity equation are neglected and the mode of disturbance is unchanged by generation shifting. The sensitivity equation of the energy margin, ΔV, caused by generation shifting can be approximated as follows [47].

$$\Delta(\Delta V) \approx \sum_{k=1}^{n} \frac{\partial(\Delta V)}{\partial P_{mk}}\Delta P_{mk}, \tag{3.3}$$

where ΔP_{mk} is the change of mechanical power input at machine k and n is the number of machines at which generator outputs are adjusted.

Once the output power of machine k is shifted, the sensitivity of the energy margin is

calculated by the partial derivative of ΔV with respect to P_{mk} [48]:

$$\begin{aligned}\frac{\partial(\Delta V)}{\partial P_{mk}} &= -M_{eq}\tilde{\omega}_{eq}^{cl}\dot{u}_{eq,k}^{cl} - (\tilde{\delta}_k^u - \tilde{\delta}_k^{cl}) - \sum_{i=1}^{n}(P_{mi} - G_{ii}|E_i|^2)(u_{ik}^u - u_{ik}^{cl}) \\ &+ \sum_{i=1}^{n-1}\sum_{j=i+1}^{n} C_{ij}[\sin\tilde{\delta}_{ij}^u(u_{ik}^u - u_{jk}^u) - \sin\tilde{\delta}_{ij}^{cl}(u_{ik}^{cl} - u_{jk}^{cl})] \\ &+ \sum_{i=1}^{n-1}\sum_{j=i+1}^{n} D_{ij}(\sin\tilde{\delta}_{ij}^u - \sin\tilde{\delta}_{ij}^{cl})[\frac{(u_{ik}^u + u_{jk}^u - u_{ik}^{cl} - u_{jk}^{cl})}{\tilde{\delta}_{ij}^u - \tilde{\delta}_{ij}^{cl}} \\ &- \frac{(u_{ik}^u - u_{jk}^u - u_{ik}^{cl} + u_{jk}^{cl})(\tilde{\delta}_i^u + \tilde{\delta}_j^u - \tilde{\delta}_i^{cl} - \tilde{\delta}_j^{cl})}{(\tilde{\delta}_{ij}^u - \tilde{\delta}_{ij}^{cl})^2}] \\ &+ \sum_{i=1}^{n-1}\sum_{j=i+1}^{n} \frac{(\tilde{\delta}_i^u + \tilde{\delta}_j^u - \tilde{\delta}_i^{cl} - \tilde{\delta}_j^{cl})}{(\tilde{\delta}_{ij}^u - \tilde{\delta}_{ij}^{cl})} D_{ij}[\cos\tilde{\delta}_{ij}^u(u_{jk}^u - u_{jk}^u) - \cos\tilde{\delta}_{ij}^{cl}(u_{ik}^{cl} - u_{jk}^{cl})] \\ &+ 2\sum_{i=1}^{n}|E_i|\frac{\partial|E_i|}{\partial P_{mk}}G_{ii}(\tilde{\delta}_i^u - \tilde{\delta}_i^{cl}) \\ &- \sum_{i=1}^{n-1}\sum_{j=i+1}^{n}(\frac{\partial|E_i|}{\partial P_{mk}}|E_j| + \frac{\partial|E_j|}{\partial P_{mk}}|E_i|)B_{ij}(\cos\tilde{\delta}_{ij}^u - \cos\tilde{\delta}_{ij}^{cl}) \\ &+ \sum_{i=1}^{n-1}\sum_{j=i+1}^{n}[G_{ij}(\frac{\partial|E_i|}{\partial P_{mk}}|E_j| + \frac{\partial|E_j|}{\partial P_{mk}}|E_i|)\frac{\tilde{\delta}_i^u + \tilde{\delta}_j^u - \tilde{\delta}_i^{cl} - \tilde{\delta}_j^{cl}}{\tilde{\delta}_{ij}^u - \tilde{\delta}_{ij}^{cl}}(\sin\tilde{\delta}_{ij}^u - \cos\tilde{\delta}_{ij}^{cl}),\end{aligned} \tag{3.4}$$

where
$\dot{u}_{eq,k}^{cl} = \dot{u}_{cr,k}^{cl} - \dot{u}_{sys,k}^{cl}$,
$\dot{u}_{cr,k}^{cl} = \frac{1}{M_{cr}}\sum_{i\in cr} M_i\dot{u}_{ik}^{cl}$,
$\dot{u}_{sys,k}^{cl} = \frac{-1}{M_T - M_{cr}}\sum_{i\in cr} M_i\dot{u}_{ik}^{cl}$,
$u_{ik}^u = \frac{\partial\tilde{\delta}_i^u}{\partial P_{mk}}$ is UEP sensitivity coefficient,
$u_{ik}^{cl} = \frac{\partial\tilde{\delta}_i^{cl}}{\partial P_{mk}}$ is clearing angle sensitivity coefficient,
$\dot{u}_{ik}^{cl} = \frac{\partial\tilde{\omega}_i^{cl}}{\partial P_{mk}}$ is clearing speed sensitivity coefficient.

The process to derive the above mentioned variables is as follows [48].

Sensitivity analysis of the speed and clearing angle:

Starting from swing equations during the faulted period,

$$M_i\dot{\tilde{\omega}}_i = P_i - P_{ei} - \frac{M_i}{M_T}P_{COI}, \quad \text{for } i = 1, n-1. \tag{3.5}$$

By differentiating equation (3.5) with respect to P_{mk}, the set of differential equations are given by [48]:

$$M_i\frac{d^2}{dt^2}u_{ik} = -Q^f_{ik} + \sum_{j=1}^{n} A^f_{ij}u_{jk}, \quad \text{for } i = 1, n-1, \tag{3.6}$$

where

$$\begin{aligned}
A^f_{ii} &= (1 - \frac{2M_i}{M_T})\sum_{\substack{j=1\\ j\neq i}}^{n} D^f_{ij}\sin\tilde{\delta}_{ij} - \sum_{\substack{j=1\\ j\neq i}}^{n} C^f_{ij}\cos\tilde{\delta}_{ij},\\
A^f_{ij} &= C^f_{ij}\cos\tilde{\delta}_{ij} - D^f_{ij}\sin\tilde{\delta}_{ij} + \frac{2M_i}{M_T}\sum_{\substack{l=1\\ l\neq j}}^{n} D^f_{lj}\sin\tilde{\delta}_{lj},\\
Q^f_{ik} &= \frac{M_i}{M_T} - \theta_{ik}\\
&\quad + \sum_{j=1}^{n}(\frac{\partial|E_i|}{\partial P_{mk}}|E_j| + \frac{\partial|E_j|}{\partial P_{mk}}|E_i|)(B^f_{ij}\sin\tilde{\delta}_{ij} + G^f_{ij}\cos\tilde{\delta}_{ij})\\
&\quad - \frac{M_i}{M_T}\sum_{j=1}^{n}\sum_{l=1}^{n}(\frac{\partial|E_l|}{\partial P_{mk}}|E_j| + \frac{\partial|E_j|}{\partial P_{mk}}|E_l|)G^f_{lj}\cos\tilde{\delta}_{lj},\\
\theta_{ik} &= 1 \text{ for } i = k,\\
\theta_{ik} &= 0 \text{ for } i \neq k.
\end{aligned}$$

The solution of the dynamic sensitivity equation can be obtained if the initial conditions are given. The initial conditions are defined based on the assumption that the angular positions and machine speeds do not change instantly. As a result, the initial conditions for u_{ik} and $\dot{u}_{ik}$ with $i = 1, n$ and $k = 1, n-1$ are given by:

$$u_{ik}(0) = u^s_{ik}, \tag{3.7}$$

$$\dot{u}_{ik}(0) = 0, \tag{3.8}$$

where the superscript s denotes the pre-fault SEP. The initial values for u_{nn} and $\dot{u}_{nn}$ are calculated by using the following equations:

$$\sum_{i=1}^{n} M_i\frac{\partial\tilde{\delta}_i}{\partial P_{mk}} = 0, \tag{3.9}$$

$$\sum_{i=1}^{n} M_i \frac{\partial \tilde{\omega}_i}{\partial P_{mk}} = 0. \tag{3.10}$$

After getting the initial conditions, the set of second order differential equations is solved to obtain clearing angles sensitivity u_{ik}^{cl} and speed sensitivity $\dot{u}_{ik}^{cl}$.

Sensitivity analysis of SEP and controlling UEP:

From the dynamic sensitivity equation, SEP sensitivity $\frac{\partial \tilde{\delta}_i^s}{\partial P_{mk}}$ can be calculated by eliminating the term $M_i \frac{d^2}{dt^2} u_{ik}$. As the system is in pre-fault condition, the pre-fault network parameters are utilized. The set of $(n-1)$ linear equations with n variables is given as:

$$\sum_{j=1}^{n} A_{ij}^{pr} u_{jk}^{s} = Q_{ik}^{pr}, \quad \text{for } i = 1, n-1, \tag{3.11}$$

where A and Q matrices are calculated using the same concept of (3.6) except that all the parameters are in pre-fault conditions (the superscript pr denote the pre-fault condition). The equation (3.9) is the n^{th} equation of the set to solve for n variables.

Controlling UEP sensitivity equations can be obtained by modifying SEP sensitivity equations by replacing the superscript s to u and changing the pre-fault conditions to post-fault conditions. The set of equations for controlling UEP sensitivity calculation is given as follows.

$$\sum_{j=1}^{n} A_{ij}^{f} u_{jk}^{u} = Q_{ik}^{f}, \quad \text{for } i = 1, n-1. \tag{3.12}$$

Similar to the SEP sensitivity equations, the n^{th} equation of the controlling UEP sensitivity equations also can be obtained from (3.9).

3.1.2 Generation Shifting and Line Distribution Factors

To calculate distribution factors of transmission lines due to generation shifting, the AC load flow is linearized to a DC load flow. With the assumption that line reactances are much larger than line resistances, the following approximations are developed [49]:

$$|E_i| = |E_j| = 1, \tag{3.13}$$

$$G_{ij} = \frac{r_{ij}}{r_{ij}^2 + x_{ij}^2} \approx 0, \tag{3.14}$$

$$B_{ij} = \frac{-x_{ij}}{r_{ij}^2 + x_{ij}^2} = \frac{-1}{x_{ij}}, \tag{3.15}$$

$$\cos(\delta_i - \delta_j) \approx 1, \tag{3.16}$$

$$\sin(\delta_i - \delta_j) \approx \delta_i - \delta_j. \tag{3.17}$$

These conditions are applied to calculate all bus phase angles in a network.

$$P_i = \sum_{j=1}^{m} P_{ij} = \sum_{j=1}^{m} \frac{1}{x_{ij}}(\delta_i - \delta_j). \tag{3.18}$$

Then,

$$P = B_x \times \delta, \tag{3.19}$$

where

$$\begin{aligned}
P &= [P_1, P_2, \ldots P_m]^T, \\
\delta &= [\delta_1, \delta_2, \ldots \delta_m]^T, \\
B_{xii} &= \sum_{j=1}^{m} \frac{1}{x_{ij}} \text{ for } i \neq \text{reference bus}, \\
B_{xii} &= 0 \text{ for } i = \text{reference bus}, \\
B_{xij} &= \frac{-1}{x_{ij}} \text{ for } i \text{ and } j \neq \text{reference bus}, \\
B_{xij} &= 0, \quad \text{for } i = \text{reference bus and } j = \text{reference bus}.
\end{aligned}$$

Using (3.19), bus phase angles are calculated as follows [49].

$$\delta = X \times P. \tag{3.20}$$

These steps help in generating matrix X. In calculating the generation shifting sensitivity factors for the generator on bus i, the perturbation on bus i is set to 1 and on the other buses are set to 0. The change in bus phase angles are as follows [49]:

$$\Delta\delta = X \begin{bmatrix} 0 \\ +1 \\ 0 \\ -1 \\ 0 \\ 0 \end{bmatrix}, \tag{3.21}$$

where $+1$ is in row i, -1 is in the reference row and other rows are zeros.

From (3.21), the distribution factor of line ℓ due to generation shift at generator i is given as follows [49].

$$\begin{aligned}
S_{\ell i} = \frac{df_\ell}{dP_i} &= \frac{d}{dP_i}\left(\frac{1}{x_\ell}(\delta_n - \delta_m)\right) \\
&= \frac{1}{x_\ell}\left(\frac{d\delta_n}{dP_i} - \frac{d\delta_m}{dP_i}\right) \\
&= \frac{1}{x_\ell}\left(X_{ni} - X_{mi}\right),
\end{aligned} \tag{3.22}$$

where X_{ni} and X_{mi} are the n^{th} and m^{th} elements of the $\Delta\delta$ matrix, respectively, and x_ℓ is the reactance of the line ℓ.

The linear relationship between line power flow changes and generation shifting is given by [49],

$$\Delta I_w = \sum_{k=1}^{n-1} S_{wk} \Delta P_{mk} \quad \text{for } k = 1, n-1, \tag{3.23}$$

where w is the monitored line.

3.2 Preventive Actions Based on Generation Shifting

If the power system is initial operating in a balanced condition and a predicted contingency makes the system unstable, preventive actions is implemented to change system's initial condition to make the system stable if the contingency occurs. In most cases, generation shifting is the appropriate preventive action. The criteria of identifying preventive actions is based on the changes in generation to make the energy margin zero or positive. The sensitivity of the energy margin with respect to the generation rescheduling is used with optimization technique to define the preventive actions.

The preventive action scheme works in two stages. It starts with scanning all possible scenarios and classifies them into stable and unstable scenarios based on the energy margin. The second stage performs optimization for unstable contingencies to choose the most effective rescheduling. Three questions are usually brought up for the cases where generation redispatch is needed [32]: (1) Which generator is rescheduled? (2) How to determine changing the setting of each generator? And (3) do these changes introduce any violation in generator and transmission line constraints. These questions can be formulated as an optimization problem as follows [50].

$$\min \{Z = (F_1, F_2, ..., F_{N+L}\}, \tag{3.24}$$

subject to:

$$g(F_i) \geq 0,$$
$$h(F_i) = 0.$$

Equality constraints in the optimization problem are usually from the power flow equations. Inequality constraints relate to branch flow limits, bus voltage magnitude limits, and generation shifting limits. In particular, the objective of the preventive action is to minimize the generation shifting and the changes of line power flow while satisfying the constraints of generation and transmission line limits to increase system energy margin:

$$F_{min} \leq F \leq F_{max}.$$

The sensitivity and distribution factor equations can be included in a matrix form to form a constraint of the optimization problem:

$$A \times F = B,$$

where Z is a vector of $N + L$ objective function, F_{min} and F_{max} are the limits of F.

$$A = \begin{bmatrix} \frac{\partial(\Delta V)}{\partial P_{m1}} & \dots & \frac{\partial(\Delta V)}{\partial P_{mn}} & 0 & \dots & 0 \\ S_{11} & \dots & S_{1n} & -1 & \dots & 0 \\ \cdot & & \cdot & & & \\ \cdot & & \cdot & & & \\ \cdot & & \cdot & & & \\ S_{L1} & \dots & S_{Ln} & 0 & \dots & -1 \end{bmatrix},$$

$$B = [\Delta(\Delta V) \quad 0 \quad \dots \quad 0]^T,$$

$$F = [\Delta P_{m1} \quad \dots \quad \Delta P_{mn} \quad \Delta I_1 \quad \dots \quad \Delta I_L]^T,$$
$$\Delta(\Delta V) = \Delta V_{new} - \Delta V_{old},$$

Solution of the optimization problem defined by equation (3.24) yield the necessary generation shifting that increases the energy margin to zero or a positive value.

3.3 Corrective Actions

Although preventive action schemes help in avoiding unstable states, which are results of disturbances, it is possible that the power system may experience an unexpected unstable state. The first reason is that not all preventive actions are applied in system operation because they might be economically expensive. Preventive actions application has to compromise with economic dispatch to ensure the most effective operation of the system. The second reason is that some preventive actions can not be implemented because there is not feasible solution for optimization problem. The third reason is that many disturbances are results of natural and random events such as broken trees or animal or lightening which usually are not included in the designated list of contingencies. In case of occurrence of an unexpected contingency the corrective action control should be able to inhibit system from cascading failure. Two types of corrective actions are considered in this project are generation tripping and load shedding. The purpose of these actions is to improve energy margin of the system from negative value to zero or positive value. It is assumed that the mode of disturbance is unchanged due to the corrective actions.

3.3.1 Generation Tripping

Corrective actions are needed if the energy margin is negative after the disturbance. It is assumed that only a small amount of generation is tripped at node k to improve the system stability. As the change in ΔP_{mk} is small compared to the total system generation (which also means a negligible amount of inertia is tripped), the parameters B_{ij}, G_{ij}, $\tilde{\delta}_0$, $\tilde{\delta}^{cl}$ do not change. Only Y_{kk} (element kk of the admittance matrix) changes due to the change in x'_{dk}

(the d - axis transient reactance of generator k) and also $\tilde{\delta}^u$ and M_{eq} [32]. The change in M_{eq} can be expressed as follows [32]:

$$\frac{\Delta M_{eq}}{\Delta P_{mk}} = \frac{M_k}{P_{mk}}. \tag{3.25}$$

The mismatch function of machine i can be expressed as follows [32].

$$f_i = P_{mi} - P_{ei} = P_{mi} - E_i^2 G_{ii} - \sum_{j \neq i} (C_{ij} \sin \tilde{\delta}_{ij} + D_{ij} \cos \tilde{\delta}_{ij}). \tag{3.26}$$

where C_{ij} and D_{ij} are as defined for (2.10).

Therefore, the change in the mismatch function can be expressed as follows:

$$\Delta f_i = -E_i^2 \Delta G_{ii} - \sum_{j \neq i} (\Delta C_{ij} \sin \tilde{\delta}_{ij} + \Delta D_{ij} \cos \tilde{\delta}_{ij}). \tag{3.27}$$

If J is the Jacobian at the equilibrium point without generation tripping, the first estimate of the change in the equilibrium point is given by [32]:

$$\begin{pmatrix} \Delta\tilde{\delta}_1 \\ \vdots \\ \Delta\tilde{\delta}_k \\ \vdots \\ \Delta\tilde{\delta}_n \end{pmatrix} = J^{-1} \begin{pmatrix} 0 \\ \vdots \\ \Delta P_{mk} \\ \vdots \\ 0 \end{pmatrix}. \tag{3.28}$$

In other words, the change in the mismatch functions, Δf_i, equal to zero for $i \neq k$ and equal to ΔP_{mk} for $i = k$. The accuracy of $\Delta\tilde{\delta}$ can be improved if the Jacobian is redefined at the new value of $\Delta\tilde{\delta}$, and then the inverse of this Jacobian is used to recalculate $\Delta\tilde{\delta}$. After determining $\Delta\tilde{\delta}^u$, the change in energy margin is given as [32]:

$$\frac{\Delta(\Delta V)}{\Delta P_{mk}} = \frac{\partial(\Delta V)}{\partial M_{eq}} \frac{\Delta M_{eq}}{\Delta P_{mk}} + \sum_{i=1}^{n} \frac{\partial(\Delta V)}{\partial \tilde{\delta}_i^u} \frac{\Delta \tilde{\delta}_i^u}{\Delta P_{mk}} + \frac{\partial(\Delta V)}{\partial P_{ik}} \frac{\Delta P_{ik}}{\Delta P_{mk}}, \tag{3.29}$$

where

$$\frac{\partial(\Delta V)}{\partial M_{eq}} = \frac{1}{2} (\tilde{w}_{eq}^{cl})^2, \tag{3.30}$$

$$\frac{\partial(\Delta V)}{\partial P_{ik}} = -(\tilde{\delta}_k^u - \tilde{\delta}_k^{cl}), \tag{3.31}$$

$$\frac{\partial(\Delta V)}{\partial \tilde{\delta}_i^u} = -P_i + \sum_{j=i+1}^{n} \left[C_{ij} \sin \tilde{\delta}_{ij}^u - D_{ij} \left(\left(\sin \tilde{\delta}_{ij}^u - \sin \tilde{\delta}_{ij}^{cl} \right) \frac{\tilde{\delta}_{ij}^u - \tilde{\delta}_{ij}^{cl} - \tilde{\delta}_{i+j}^u + \tilde{\delta}_{i+j}^{cl}}{\left(\tilde{\delta}_{ij}^u - \tilde{\delta}_{ij}^{cl} \right)^2} + \frac{\tilde{\delta}_{i+j}^u - \tilde{\delta}_{i+j}^{cl}}{\tilde{\delta}_{ij}^u - \tilde{\delta}_{ij}^{cl}} \cos \tilde{\delta}_{ij}^u \right) \right]. \tag{3.32}$$

After generation tripping, the new value of M_{eq} and $\tilde{w}_{eq}$ are $\hat{M}_{eq}$ and $\hat{w}_{eq}$ which can be calculated as follows [32].

$$\hat{M}_{eq} = (1 - K)M_{eq}, \tag{3.33}$$

$$\hat{w}_{eq} \simeq \tilde{w}_{eq} + K(\tilde{w}_{cr} - \tilde{w}_k), \tag{3.34}$$

where $K = \frac{\Delta M_k}{M_{cr}}$. The change of ΔV due to generation tripping is given by [32]:

$$\Delta(\Delta V) = \Delta V_{KE} + \Delta V_{PE} + \Delta V_{ME} + \Delta V_{DE}, \tag{3.35}$$

where

$$\Delta V_{KE} = \frac{1}{2}(\hat{M}_{eq}\hat{w}_{eq}^2 - M_{eq}\tilde{w}_{eq}^2), \tag{3.36}$$

$$\Delta V_{PE} = -P_{ko}\Delta\tilde{\delta}_k^u - \Delta P_k\tilde{\delta}_{ko}^u - \Delta P_k\Delta\tilde{\delta}_k^u - \sum_{i\neq k} P_{io}\Delta\tilde{\delta}_i^u, \tag{3.37}$$

$$\Delta V_{ME} = -\sum_{i=1}^{n-1}\sum_{j=i+1}^{n} C_{ij}\sin\tilde{\delta}_{ijo}^u\Delta\tilde{\delta}_{ij}^u, \tag{3.38}$$

$$\Delta V_{DE} = -\sum_{i=1}^{n-1}\sum_{j=i+1}^{n} D_{ij}\Delta\tilde{\delta}_{ij}^u \left[\frac{\tilde{\delta}_{ijo}^u - \tilde{\delta}_{ij}^{cl} - \tilde{\delta}_{i+jo}^u + \tilde{\delta}_{i+j}^{cl}}{\left(\tilde{\delta}_{ijo}^u - \tilde{\delta}_{ij}^{cl}\right)^2}\left(\sin\tilde{\delta}_{ijo}^u - \sin\tilde{\delta}_{ij}^{cl}\right) + \frac{\tilde{\delta}_{i+jo}^u - \tilde{\delta}_{i+j}^{cl}}{\tilde{\delta}_{ijo}^u - \tilde{\delta}_{ij}^{cl}}\left(\cos\tilde{\delta}_{ijo}^u - \cos\tilde{\delta}_{ij}^u\right)\right]. \tag{3.39}$$

The subscripts KE, PE, ME, and DE stand for kinetic energy, position energy, magnetic energy and dissipation energy, respectively.

3.3.2 Load Rejection

Load rejection is expressed by a change in the impedance of load buses (Y_{bus} matrix changes). Hence, the $\tilde{\delta}^u$ changes as well but there is no change in P_{mi} and M_i. The energy margin changes due to the change in potential energy.

The change in $\Delta\tilde{\delta}^u$ due to load rejection is expressed as [32]:

$$\begin{pmatrix} \Delta\tilde{\delta}_1^u \\ \Delta\tilde{\delta}_2^u \\ \vdots \\ \Delta\tilde{\delta}_n^u \end{pmatrix} = J^{-1}\begin{pmatrix} \Delta f_1 \\ \Delta f_2 \\ \vdots \\ \Delta f_n \end{pmatrix}, \tag{3.40}$$

where

$$\frac{\Delta(\Delta V)}{\Delta G_{ii}} = \frac{\partial(\Delta V)}{\partial P_i}\frac{\Delta P_i}{\Delta G_{ii}} + \sum_{i=1}^{n}\frac{\partial(\Delta V)}{\partial \tilde{\delta}_i^u}\frac{\Delta \tilde{\delta}_{i,G_{ii}}^u}{\Delta G_{ii}} = (\tilde{\delta}_{io}^u - \tilde{\delta}_{io}^{cl})(-E_i^2) + \tilde{\delta}_{io}^u\frac{\Delta \tilde{\delta}_{i,G_{ii}}^u}{\Delta G_{ii}}, \quad (3.41)$$

$$\frac{\partial(\Delta V)}{\partial \tilde{\delta}_i^u} = -P_i + \sum_{j=i+1}^{n}\left[C_{ijo}\sin\tilde{\delta}_{ij}^u - D_{ij}\left(\left(\sin\tilde{\delta}_{ij}^u - \sin\tilde{\delta}_{ij}^{cl}\right)\frac{\tilde{\delta}_{ij}^u - \tilde{\delta}_{ij}^{cl} - \tilde{\delta}_{i+j}^u + \tilde{\delta}_{i+j}^{cl}}{\left(\tilde{\delta}_{ij}^u - \tilde{\delta}_{ij}^{cl}\right)^2} + \frac{\tilde{\delta}_{i+j}^u - \tilde{\delta}_{i+j}^{cl}}{\tilde{\delta}_{ij}^u - \tilde{\delta}_{ij}^{cl}}\cos\tilde{\delta}_{ij}^u\right)\right], \quad (3.42)$$

$$\frac{\partial(\Delta V)}{\partial C_{ij}} = \frac{\partial(\Delta V)}{\partial \tilde{\delta}_i^u}\frac{\Delta \tilde{\delta}_{i,C_{ij}}^u}{\Delta C_{ij}}, \quad (3.43)$$

$$\frac{\partial(\Delta V)}{\partial D_{ij}} = \frac{\partial(\Delta V)}{\partial \tilde{\delta}_i^u}\frac{\Delta \tilde{\delta}_{i,D_{ij}}^u}{\Delta D_{ij}}, \quad (3.44)$$

$$\Delta(\Delta V) = \frac{\partial(\Delta V)}{\partial G_{ii}}\Delta G_{ii} + \frac{\partial(\Delta V)}{\partial C_{ij}}\Delta C_{ij} + \frac{\partial(\Delta V)}{\partial D_{ij}}\Delta D_{ij}, \quad (3.45)$$

and $\Delta\tilde{\delta}_{i,G_{ii}}^u$, $\Delta\tilde{\delta}_{i,C_{ij}}^u$, and $\Delta\tilde{\delta}_{i,D_{ij}}^u$ are the change in $\Delta\tilde{\delta}_i^u$ due to the change in G_{ii}, C_{ij}, and D_{ij}, respectively.

Again, the accuracy of $\Delta\tilde{\delta}$ can be improved if the Jacobian J at $(\tilde{\delta}^u + \Delta\tilde{\delta}^u)$ is recalculated and then $\Delta\tilde{\delta}^u$ is determined.

3.3.3 Application of Braking Resistor

The effect of applying a braking resistor is opposite to that of load shedding [32]. Similar to the load shedding, the variation in ΔV is determined by defining the change in the elements of Y_{bus} and then $\Delta\tilde{\delta}_i^u$ and ΔV.

4. Trajectory Correction Using Real-time Data

As the screening tools are operating in real time, obtaining the real-time data of the system is very important. The continuous updating data improves the accuracy of transient screening and remedial actions tools. The real-time data collection is implemented by Supervisory Control and Data Acquisition (SCADA) measurements or the phasor measurement units (PMU). The obtained real-time data is the raw input for the screening tools and often doesn't include all the necessary data input for the screening process. Therefore, another procedure is needed to analyze this raw data: state estimation. As PMUs have advantage of incorporating phase angle measurements and these measurements are synchronized and time stamped, which increase the state estimation accuracy and reliability, they are considered in this project. Moreover, the introduction of PMU makes the state estimation no longer a linear problem. The data streaming is retrieved using OpenPDC and the Microsoft SQL Server database. The process to obtain the real-time data from PMU and the state estimation is presented as follows.

4.1 Real-Time Data Streaming

4.1.1 OpenPDC

A Phasor Data Concentrator (PDC) was set up at CAPS laboratory. For this, we have used open source software called "Open PDC" [51]. This software runs in windows platform and can be used with SQL Server, MySQL or MS Access Database system as data historian. Fig. 4.1 shows the home screen of Open PDC manager software. In our setup, we used "Microsoft SQL server 2012" software to store phasor data. The OpenPDC software system can process streaming time-series data in real-time and can also store in a database format that is configured during the installation of the software. Also there are several ways to export the stored data in real-time in CSV or any other format. It can also stream data out through Internet using C37.118.2-2011 protocol so that other PDC can receive these data. Several PMUs are placed on the RTDS model of the tested systems at different locations which are streaming phasor data in real-time using IEEE C37.118.2-2011 protocol over the Internet. In OpenPDC manager, we configured the IP address and relevant configuration settings for each PMU.

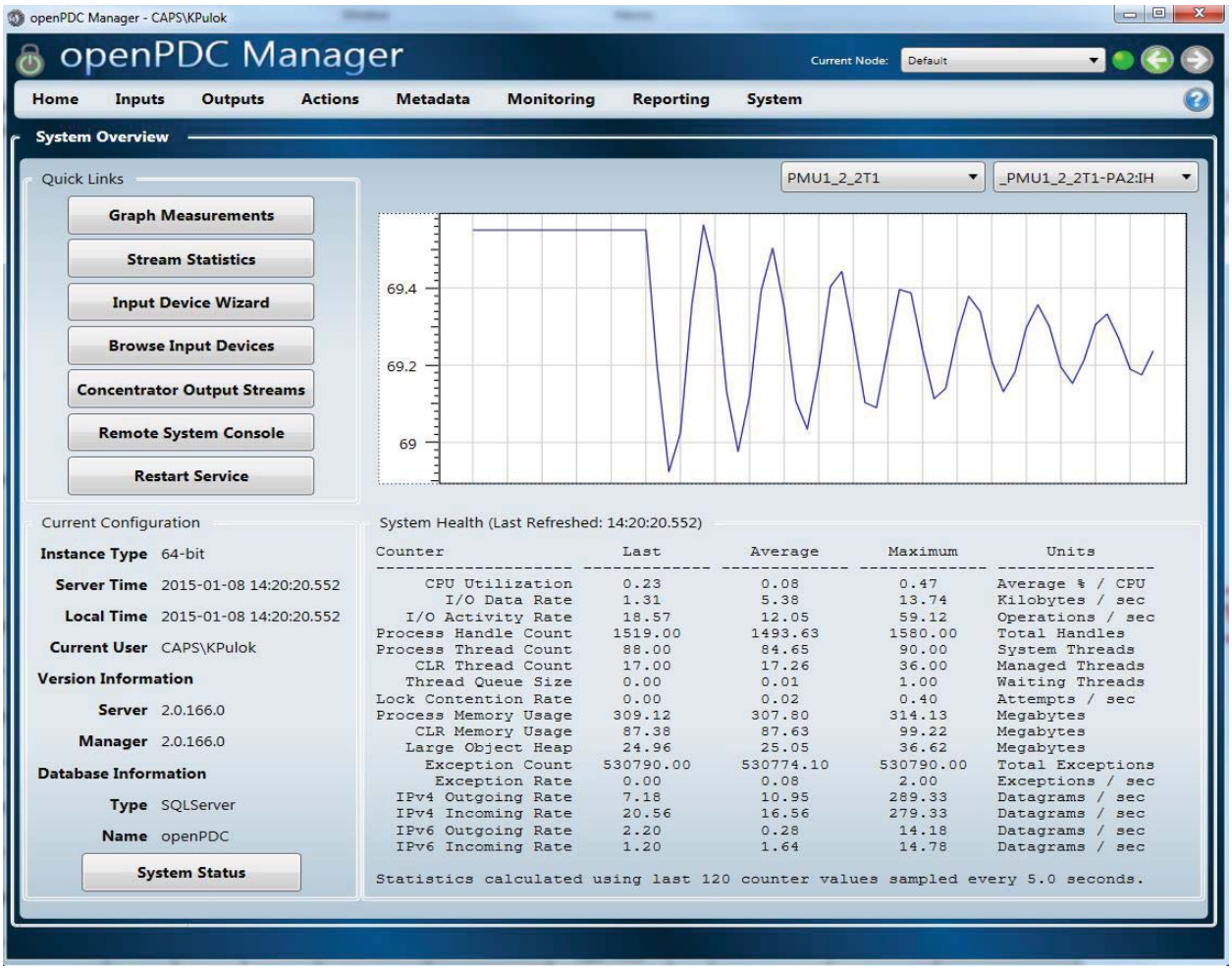

Figure 4.1: Home screen of Open PDC manager software.

4.1.2 Retrieving PMU Data from Microsoft SQL Server Database

This part mainly records how to retrieve the PMU measurements from the Microsoft SQL Server database. The streaming data from PMU are stored in a database named as openPDC. All the tables under it are related to storing data for parameters of openPDC. When the PMU devices are streaming measurement data, the phasor measurements are written into the table named TimeSeriesMeasurement, which is one of the tables in the database openPDC. The procedures are as follows,

1. Connect to the MS SQL Server, go to the database openPDC and apply DISTINCT command to select all the distinct descriptions we need in the table named dbo.Measurement.

2. Each signal ID has its unique descriptions. We need to determine the two buses which are measured by the PMU and assign a tag number for each type of signal. For example, 1 is used to represent the real part of current, 2 for the imaginary part of current, 3 for the real part of voltage and 4 for the imaginary part of voltage, etc. Thus, based on the descriptions and other documents, we are able to translate the signal ID into a readable format. Then we created a new database named SignalIDDescription in the SQL Server

and create a new table called PMUDescription in this new database. After that, import the translated descriptions with tag numbers to the table PMUDescription.

3. Select the latest measurement and write to a text file. First, we created a stored procedure spSAVEtoTXT in the database SignalIDDescription. When spSAVEtoTXT is executed, the table openPDC.dbo.TimeSeriesMeasurement and the table SignalIDDescription.dbo.PMUDescription can be combined based on matching the same signalID in the two tables.

4. Use Fortran code to retrieve the PMU measurements from MS SQL Server. In this step we need to apply BCP (bulk copy program). BCP is a utility which is installed with MS SQL Server and can assist with large data transfers.

   In general, the procedure of retrieving real-time data is as displayed in Figure 4.2.

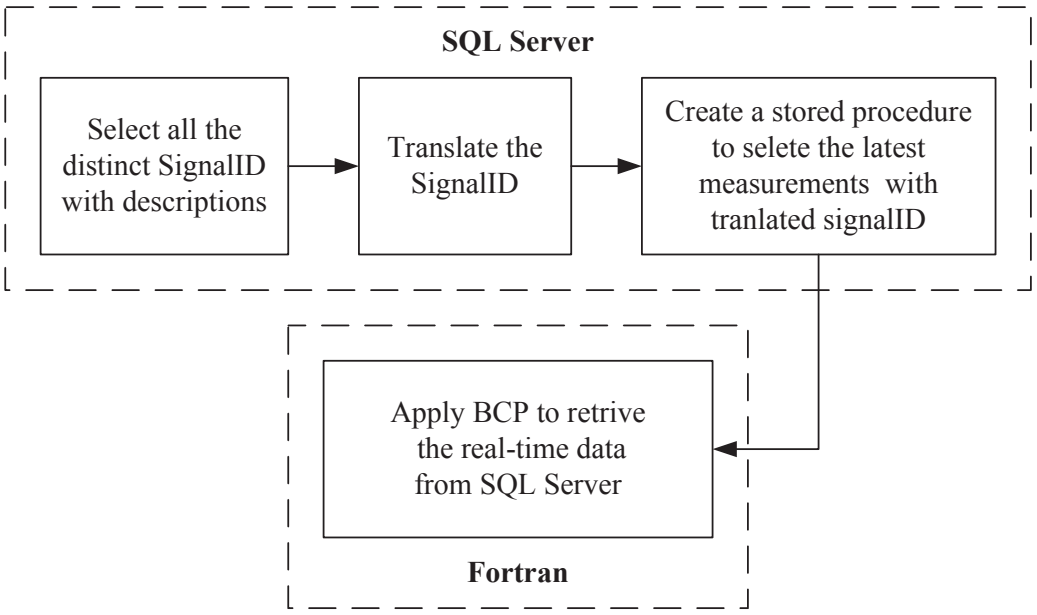

Figure 4.2: Procedure for retrieving real-time data.

4.2 State Estimation Using Phasor Measurement Units

Power system state estimation is essential for Energy Management System (EMS). It is required for real state monitoring, for optimal dispatch and for security analysis. Therefore, obtaining accurate state estimation is very significant before any security assessment or remedial action. To achieve better accuracy, the number of measurements is not restricted to merely satisfy the requirement of power flow analysis. Redundancy of measurements can

help detect bad data measurements, reduce gross errors, and provide more credible state estimations.

Traditionally, Supervisory Control and Data Acquisition (SCADA) measurements are used for power systems estimations; those measurements include voltage magnitudes, current magnitudes, real power and reactive power. However, with an emergence of phasor measurement units (PMU), state estimation became more reliable. PMUs incorporate phase angle measurements, which increase the state estimation accuracy. Moreover, these measurements are synchronized and time stamped which increase the reliability of the state estimators. In addition, using linear estimators is feasible when PMUs are used [52, 53]. Each PMU installed at a certain bus, measures the voltage phasor at that bus and also measure the currents at each branch connected to that bus [54]. As a result, estimating the static states becomes a linear problem.

4.2.1 Power System Observability

The observability of a system is determined if enough measurements have been well distributed in the system. A network is considered observable if sufficient measurements are placed to make state estimation of the system feasible. If a system is not fully observable, it is still meaningful to study whether there is a part of the system that can be observed. Observability analysis is always implemented before state estimation to check if the system states can be estimated.

A system is observable if all the flows in the network can be detected by some of the measurements, which means if there is a nonzero flow in the network, some measurements should be non-zeros. If the values of all the measurements are zeros, there should be no flows in the system.

Numerically, the observability of a network with a size of N buses can be determined using the observability test 4.1.

$$AB \geq \mathbf{I} \tag{4.1}$$

where

B = is a bus vector with length N.
A = is a connection matrix with a size of $N \times N$.
$\mathbf{I}$ = is a ones vector with length N.
N = number of buses in the system.

The elements of the bus vector B and the the connection matrix A are determined using (4.2) and (4.3).

$$b_i = \begin{cases} 1, & \text{if a PMU is installed at bus } i \\ 0, & \text{if no PMU is at that bus} \end{cases} \tag{4.2}$$

$$a_{ij} = \begin{cases} 1, & \text{if a PMU is installed at bus } i \\ 1, & \text{if there is a branch connecting bus } i \text{ and bus } j \\ 0, & \text{else} \end{cases} \tag{4.3}$$

The result from multiplying A and B in (4.1), indicates how much redundancy is presented in the network. There need to be enough redundancy in the network to handle $N-1$ contingencies. However, due to the high cost of installing PMUs, several researchers have purposed different methods for the minimal and optimal placement of PMUs [54–56]. For this project, enough PMUs were installed for each case to guarantee full observability under $N-1$ contingencies.

4.2.2 Linearized State Estimation

With the introduction of PMUs the state estimation is no longer a nonlinear problem [52,53]. As mentioned earlier, PMUs measure the voltage phasor in addition to current in phasors at the branches [55]. considering that, the measured voltage and currents can be expressed as follows:

$$V_m(k) = [V(k)_m^{real} + V(k)_m^{imag}] \tag{4.4}$$

$$I_m(k) = [I(k)_m^{real} + I(k)_m^{imag}] \tag{4.5}$$

The real and imaginary currents can be expressed using the branch admittance $G_{ij}+jB_{ij}$ and the shunt B_{ii} as

$$I_{m_{ij}}^{real} = G_{ij}[V_i(k)^{real} - V_j(k)^{real}] - B_{ij}[V_i(k)^{imag} - V_j(k)^{imag}] - B_{ii}V_i(k) \tag{4.6}$$

$$I_{m_{ij}}^{imag} = G_{ij}[V_i(k)^{imag} - V_j(k)^{imag}] - B_{ij}[V_i(k)^{real} - V_j(k)^{real}] + B_{ii}V_i(k) \tag{4.7}$$

For static estimation, the system states $X^T = [V_1^{real}\ V_1^{imag} \dots V_n^{real}\ V_n^{imag}]$ are considered to be the real and imaginary voltages at each bus in the system. The measurements signals, can be organized in a matrix as follows $Z^T = [V_i^{real}\ V_i^{imag} \dots I_m^{real}\ I_m^{imag}]$. Using those states the model can be presented as

$$Z_k = Hx_k + v_k \tag{4.8}$$

where

k = a discrete time instant.
H= a measurement matrix.
v = a measurement noise vector.

The measurement matrix H is a $(2 \times mv + 2 \times mi)$ by $(2 \times n)$ matrix defined as

$$H = \begin{bmatrix} I_{mv\times 2n} \\ h_{\alpha_1} \\ h_{\beta_1} \\ \cdot \\ \cdot \\ \cdot \\ h_{\alpha_{mi}} \\ h_{\beta_{mi}} \end{bmatrix} \tag{4.9}$$

where mv and mi are the number of voltage and current measurements respectively. h_α and h_β are the equivalent admittance row vectors obtained form (4.6) and (4.5), respectively.

$$h_\alpha = [G_{ij} \quad -G_{ij} \quad -B_{ij} - B_{ii} \quad B_{ij}]_{(1\times 2n)} \tag{4.10}$$

$$h_\beta = [-B_{ij} + B_{ii} \quad B_{ij} \quad G_{ij} \quad G_{ij}]_{(1\times 2n)} \tag{4.11}$$

The above model can be solved for the power system states X using Weighted least squares (WLS) or a modified Kalman filter. Both methods are presented in the next two sections.

WLS Method

There have been many studies on Power systems State Estimation using WLS [53, 57, 58]. The algorithm for WLS is shown as follows:

$$\begin{cases} Gm = H^T \times R^{-1} \times H \\ \hat{X} = Gm^{-1} \times H^T \times R^{-1} \times z \end{cases} \tag{4.12}$$

where H is the measurement matrix in (4.9). Since the model is linear the iterative process is eliminated and the states are estimated on the go. There is a need for a minimal post estimation analysis for bad data detection.

Kalman Filter Approach

The Kalman filter is used for estimating both the static and dynamic states [52, 59]. Considering the measurement model in (4.8) is a linear one, a regular Kalman filter can be used as follows:

$$X_k = Ax_{k-1} + Bu_{k-1} + w_{k-1} \tag{4.13}$$

$$Z_k = Hx_k + v_k \tag{4.14}$$

The Kalman estimation is done in two steps, prediction and correction. The prediction step calculates the priori state estimation as follows:

$$\begin{cases} \hat{x^-}_k = A\hat{x}_{k-1} + Bu_{k-1} \\ P_k^- = AP_{k-1}A^T + Q \end{cases} \tag{4.15}$$

The posterior or correction step is done by updating the Kalman filter gain K_k and updating the covariance P_k in (4.16).

$$\begin{cases} K_k = P_k^- H^T (HP_k^- H^T + R)^-1 \\ \hat{x}_k = \hat{x^-}_k + K_k(z_k - H\hat{x}_k^-) \\ P_k^+ = (I - K_k H)P_k^- \end{cases} \tag{4.16}$$

The obtained estimated states from (4.16), are used for power estimation and fed along with the estimated power to the transient analysis tool.

Power Estimation

The power in each bus can be estimated by using the estimated voltages. First the currents obtained form the PMUs measurements are used in (4.18). Since not all currents are measured by the PMUs, the missing currents are calculated using the estimated voltages along with the line data as in (4.17).

$$\hat{I}_{ij} = (V_i - a \times V_j) \times \frac{y_{ij}}{a_{ij}^2} + Bii \times V_i \tag{4.17}$$

where y_{ij} and a_{ij} are the line admittance and tap ratio respectively. The power flow is calculated using (4.18). After that, the power at each bus can be calculated using (4.19). It should be noted that, when the currents are estimated using the voltage estimates, the probability of error in the power calculations increases notably.

$$P_{ij} = I_{ij}^* \times \hat{V}_i \tag{4.18}$$

$$P_i = \sum_{j=1}^{N} P_{ij} \tag{4.19}$$

where

P_{ij} = the power flow between bus i and bus j.
P_i = the power at bus i.
I_{ij} = the current between bus i and bus j.
N = number of buses in the system.

5. Interactive Real-Time Transient Stability Visualization Tool

After the transient screening and remedial actions calculation, the system status and parameters are demonstrated by a visualization tool, which gives users valuable insight into the state of the network. The proposed interactive real-time visualization tool enables the selection of appropriate remedial actions that stabilize power systems due to large disturbances. Real-time data is constantly received from the PMUs so that the users can monitor bus angle, frequency, and voltage as well as power flow on the lines on a single line diagram. System status is updated both on the visualization tool and the transient screening the remedial action tools. The recommended remedial actions are also displayed on the visualization tool so that the users can decide which action should be initiated. The layout of the proposed real-time interactive visualization tool is shown in Fig. 5.1.

5.1 Tool Functions

The tool receives data, display data and suggested remedial action and initiate action. The function of the interactive visualization tool can be summarized as follows:

A. Receives measurements, fault conditions and suggested remedial action,

B. Displays the status of the system along with the suggested action,

C. Initiates an action for the faulted cases or for the preventive action,

D. Sends the control signal back to the system to perform the action.

5.2 Initiation of Remedial Actions

In addition to displaying the appropriate data, the tool displays the suggested remedial action and enable initiating control action. These actions can classified according to the time frame as follows:

A. *Fast*: (1) line tripping, (2) load shedding, (3) generation tripping,

B. *Slow*: (1) generation rescheduling, (2) voltage control, (3) reactive power control,

C. If the time allows, both the *slow* and the *fast* actions should be active. If the time is short to perform the slow actions, the slow action should be deactivated.

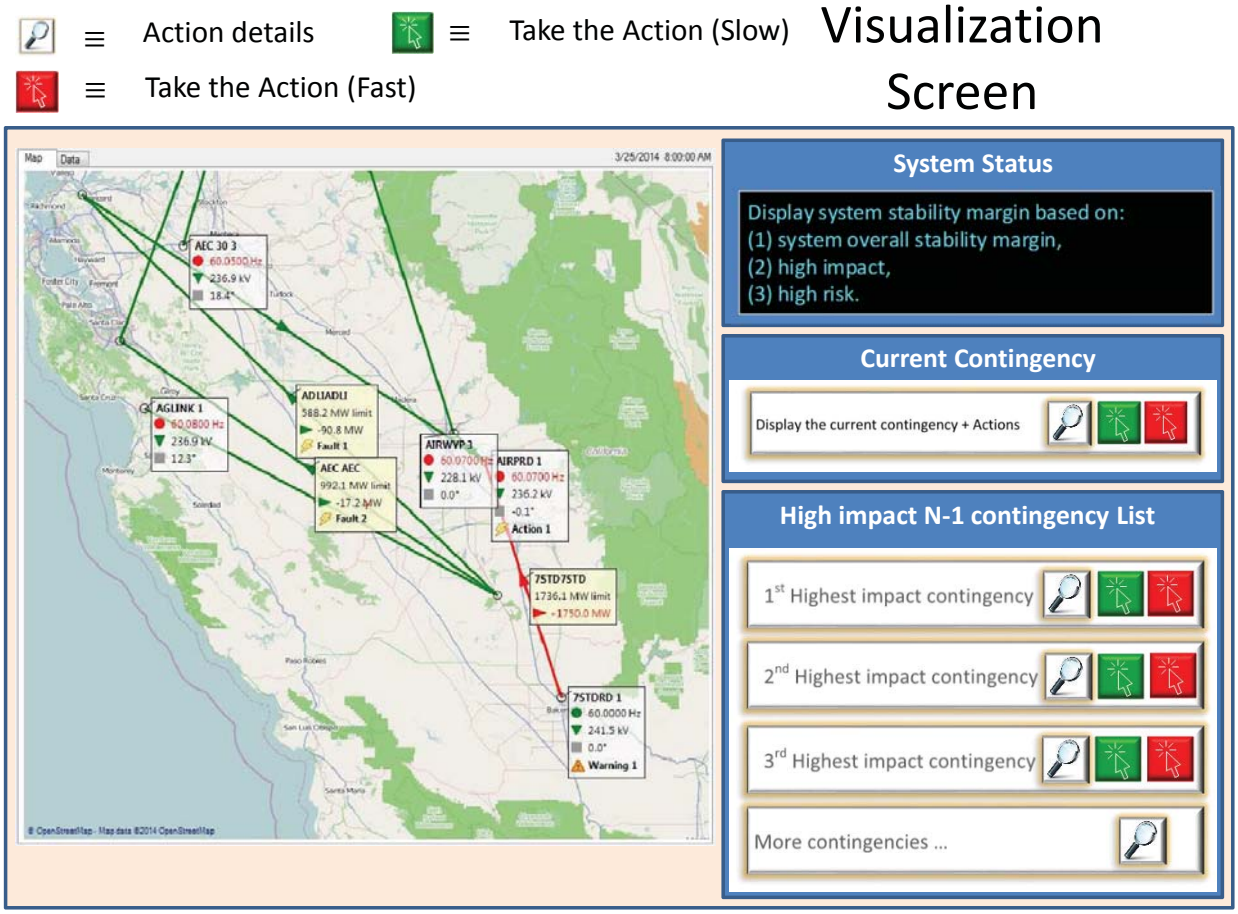

Figure 5.1: Layout of visualization tool.

5.3 System Stability Status

Several methods can be used to represent the stability status of the system. Two methods are utilized to inform the operators about the status of the system in real-time. These methods are summarized as follows:

A. Raking according to the severity. Displaying the most severe N-1 contingencies with the stability margins and the recommended action.

B. Providing a "stability index" for the current status of the system (section of Remedial Actions).

5.4 Display

In addition to displaying the voltage, frequency, angle and fault conditions and the lines and generators that reach/close to their limits, the following stability assessment indices are displayed:

A. Display the ranked contingencies (section 5.3–A) with their stability margins.

B. Display the recommended action for each contingency.

C. Display click buttons to initiate the action (for fast and slow actions).

D. Display system stability margin as an indicator.

5.5 Remedial Actions

Along with each suggested action, which could be one or more of the following: line tripping, load shedding, generation rescheduling, etc., the action ID and a flag with value 0 are sent to the visualization tool. If an action is initiated, the action ID with a flag value of 1 is sent back from the visualization tool to the LRAS tool. The flag remains 0 if no action is initiated. The ranking and list of contingencies are updated with constant frequency.

5.6 Description of Actions

- Generators: we send generator ID, location (bus) and action. Actions: 0 means trip, value means set a new operating point.
- Loads: we send load ID, location (bus) and action. Actions: 1 means shed the load.
- Lines: we send line ID, location (from bus to bus) and action. Actions: 1 means trip the line.
- Voltage control: we send device ID, location (bus) and action. Actions: the value of the new set point.

5.7 Update/Refresh Frequency

- For the preventive actions the frequency of update and data refresh does not need to be high.
- For corrective actions, the frequency should be high.

The implementation of transient screening, remedial actions, trajectory correction and visualization are presented in the next section.

5.8 Tool Description

The visualization tool application NetworkVision is developed and named by LCG to highlight its ability to give users valuable insight into the state of the network. The NetworkVision application provides a visual interface to monitor the status of the electrical network. It enables the user to constantly analyze the system status through monitoring bus angle, frequency, and voltage as well as power flow on the lines on a single line diagram.

NetworkVision has been written using the most recent version of Microsoft's powerful .NET technology, with state-of-the art coding patterns, by a team consisting of LCG's senior engineers. The application has been thoroughly tested for bugs, performance and usability. A visualization of a system is shown in Figure 5.2.

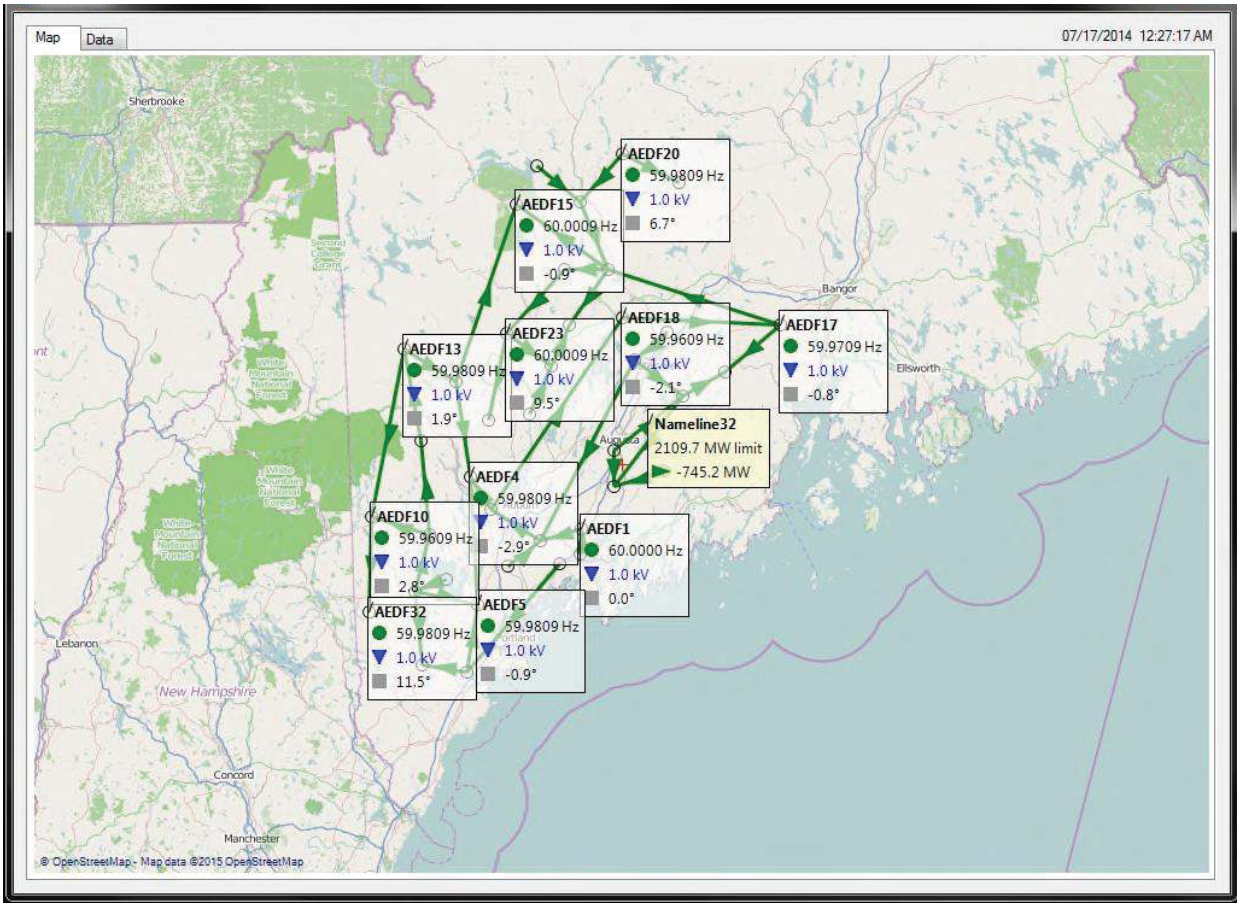

Figure 5.2: Visualization of test system.

The screen is divided into four parts: (1) the map showing the measurements, (2) a window shows system status, (3) a window shows the current contingencies if there is any, and (4) a window shows the a list possible future contingencies that are ranked according to their impact for preventive actions.

For the current and possible contingencies, there are three buttons: one to show the details (with a magnifier sign), one to take slow action (green arrow) and one to take fast actions (red arrow). For the current contingencies window, if there is no contingency, these buttons are disabled. However, if there is contingency, the detail button is active and the slow and fast action buttons are active only if it causes instability. For the possible contingencies list, all of the three buttons are active. The operator can browse the details and take an action of the possible list of contingencies at any time.

5.8.1 Reading the Diagram

The diagram displays the data superimposed on a map background, with buses being indicated by black-bordered circles displayed at their geographic location, with branches drawn as lines between them. White information boxes pointing to the buses have the bus name as the title, and show frequency, voltage and angle data using circle, triangle and square symbols, respectively. Yellow information boxes pointing to the branches show branch name, limit and actual power flow. The branch information boxes are hidden by default, but can be revealed by hovering the mouse cursor over the line. The flow direction of the branch is indicated on the line using an arrow. Note that NetworkVision contains logic to avoid information boxes overlapping each other, by removing some of the boxes where they are crowded. To see the missing boxes, the user should zoom in.

Deviant Conditions

While green represents normal conditions, other colors allow deviant conditions to be instantly recognized by the user. For frequency and angle, blue represents low values, while red represents high. For the branches, red means congested. The deviant frequencies and voltages are shown in Figure 5.3.

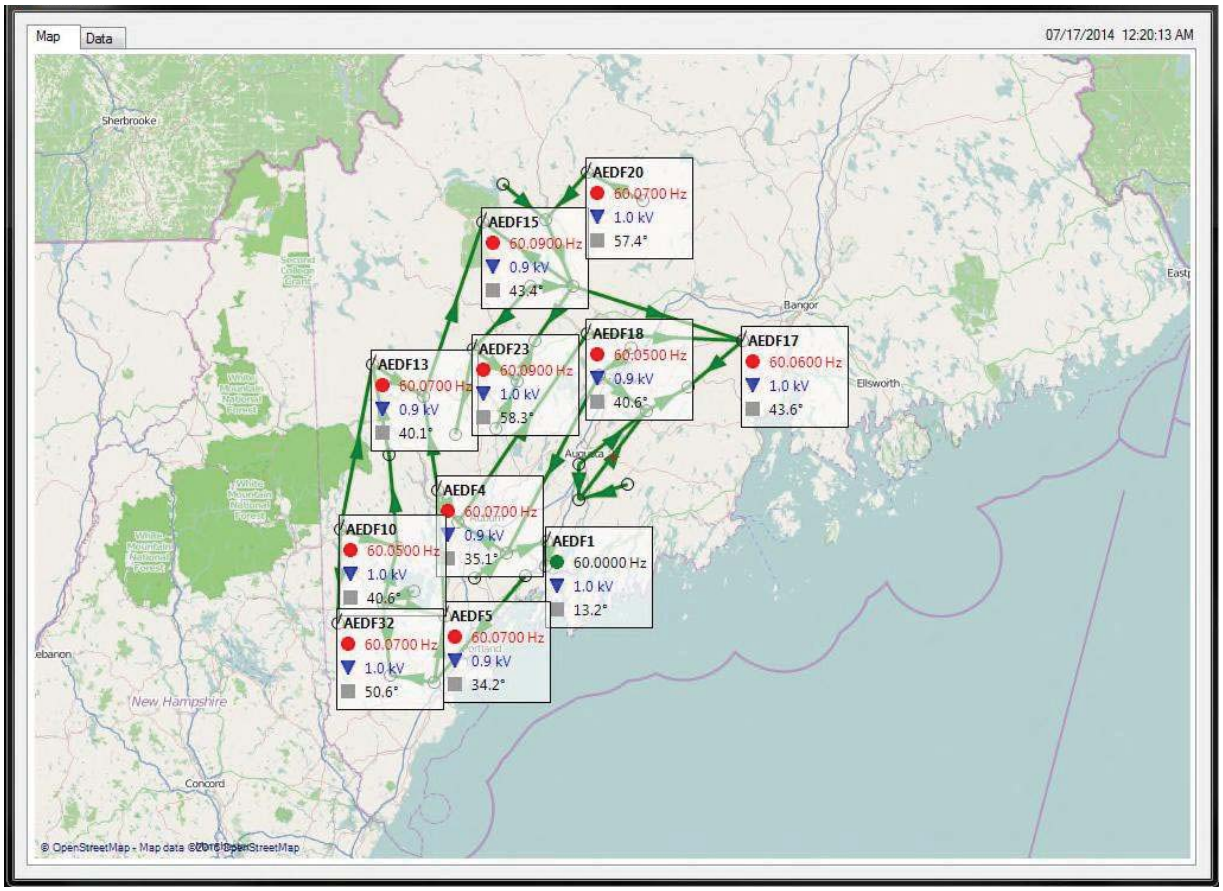

Figure 5.3: Deviant conditions of frequencies and voltages on visualization tool.

In addition, both bus and branch boxes can provide textual faults or warnings as provided in the data stream, as illustrated in Figure 5.4. The diagram key is shown in Figure 5.5.

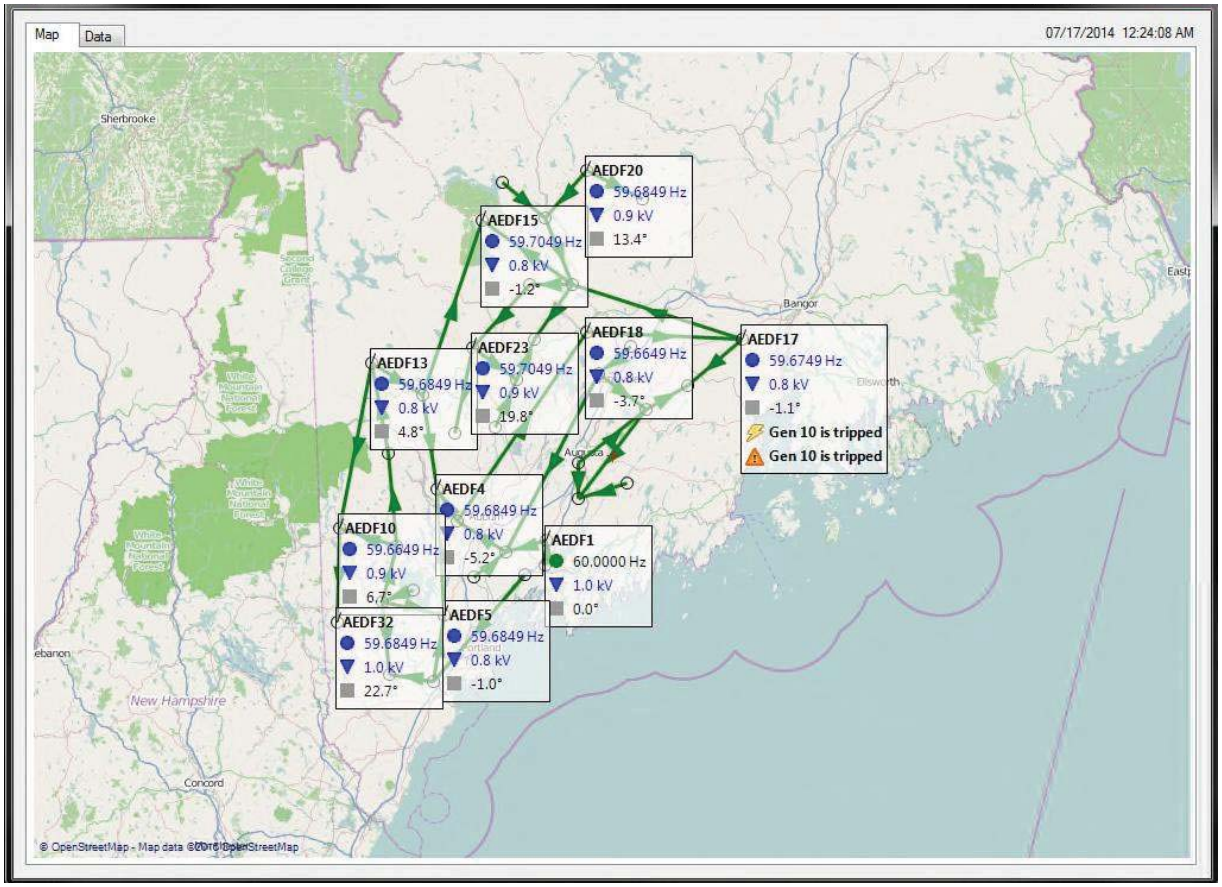

Figure 5.4: Textual faults or warnings on visualization tool.

User Interaction

The user can zoom in or out by using the mouse wheel, and pan the map by holding down the right mouse button and dragging.

Tabular View

As well as using the diagram, the user can observe data in tabular format by clicking the Data tab at the top of the screen. By selecting a value from the Table drop down list, it is possible to see the data for each of the eleven CSV files in each data stream. The tabular data for buses is shown in Figure 5.6.

NetworkVision Deployment

The *NetworkVision* package consists of an executable file that runs on a Microsoft Windows platform. It accesses data files in CSV (comma-separated values) format, stored on the local server. There are 11 files that conform to the specified format. Every time a change in

Symbol	Description
	Bus
	Branch, with flow direction
	Branch, congested
	Bus Information Box color
	Branch Information Box color
	Bus Frequency (Hz)
	Bus Frequency (Hz), low
	Bus Frequency (Hz), high
	Bus Voltage (kV)
	Bus Voltage (kV), low
	Bus Voltage (kV), high
	Bus Angle (°)
limit	Branch Flow Limit (MW)
	Branch Flow (MW)
	Fault
	Warning

Figure 5.5: The diagram key of visualization tool.

system conditions occur, the files are updated, and this triggers an update of the display on the map.

NetworkVision works by "watching" a specified folder on a computer. The user specifies the path where the data files are streamed to, in the configuration file. The data stream structure should consist of a subfolder which stores the set of 11 CSV files which have a specific naming convention and file format. If the files that are dropped in the appropriate folder, the data contained in the files appears on the diagram instantly.

Data Stream File Specifications

The following files are required for NetworkVision to read. The file format should be in CSV (comma-separated values) format and the file names and column headers should be exactly as specified. Where no data is present, empty files with column headers should be provided.

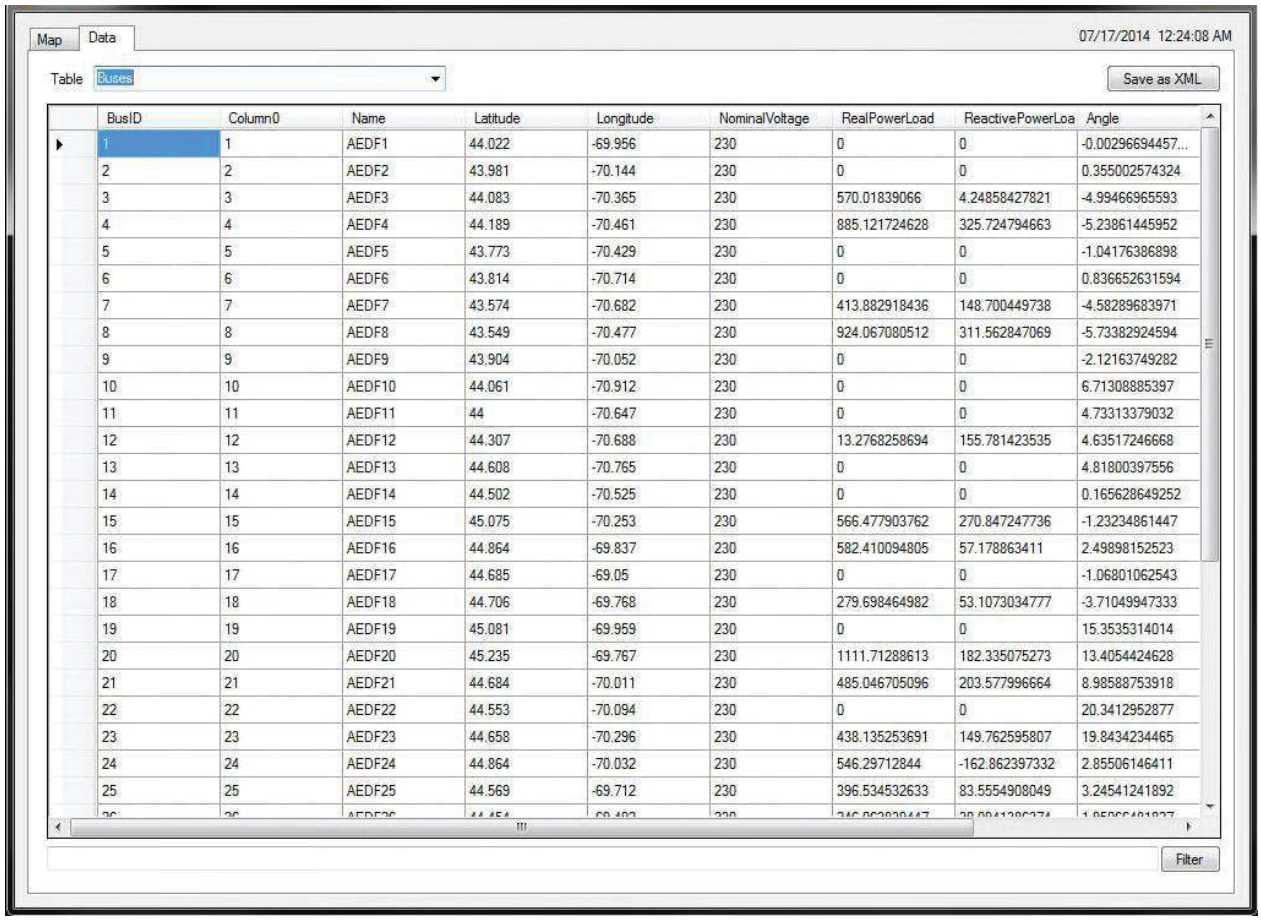

BusID	Column0	Name	Latitude	Longitude	NominalVoltage	RealPowerLoad	ReactivePowerLoa	Angle
1	1	AEDF1	44.022	-69.956	230	0	0	-0.00296694457...
2	2	AEDF2	43.981	-70.144	230	0	0	0.355002574324
3	3	AEDF3	44.083	-70.365	230	570.01839066	4.24858427821	-4.99466965593
4	4	AEDF4	44.189	-70.461	230	885.121724628	325.724794663	-5.23861445952
5	5	AEDF5	43.773	-70.429	230	0	0	-1.04176386898
6	6	AEDF6	43.814	-70.714	230	0	0	0.836652631594
7	7	AEDF7	43.574	-70.682	230	413.882918436	148.700449738	-4.58289683971
8	8	AEDF8	43.549	-70.477	230	924.067080512	311.562847069	-5.73382924594
9	9	AEDF9	43.904	-70.052	230	0	0	-2.12163749282
10	10	AEDF10	44.061	-70.912	230	0	0	6.71308885397
11	11	AEDF11	44	-70.647	230	0	0	4.73313379032
12	12	AEDF12	44.307	-70.688	230	13.2768258694	155.781423535	4.63517246668
13	13	AEDF13	44.608	-70.765	230	0	0	4.81800397556
14	14	AEDF14	44.502	-70.525	230	0	0	0.165628649252
15	15	AEDF15	45.075	-70.253	230	566.477903762	270.847247736	-1.23234861447
16	16	AEDF16	44.864	-69.837	230	582.410094805	57.178863411	2.49898152523
17	17	AEDF17	44.685	-69.05	230	0	0	-1.06801062543
18	18	AEDF18	44.706	-69.768	230	279.698464982	53.1073034777	-3.71049947333
19	19	AEDF19	45.081	-69.959	230	0	0	15.3535314014
20	20	AEDF20	45.235	-69.767	230	1111.71288613	182.335075273	13.4054424628
21	21	AEDF21	44.684	-70.011	230	485.046705096	203.577996664	8.98588753918
22	22	AEDF22	44.553	-70.094	230	0	0	20.3412952877
23	23	AEDF23	44.658	-70.296	230	438.135253691	149.762595807	19.8434234465
24	24	AEDF24	44.864	-70.032	230	546.29712844	-162.862397332	2.85506146411
25	25	AEDF25	44.569	-69.712	230	396.534532633	83.5554908049	3.24541241892

Figure 5.6: Tabular view of observed data on visualization tool.

Table 5.1: Data stream file specifications.

File name	Column headers	Data type
Bus Fault.csv	BusID	Number
	Description	String
Bus Warning.csv	BusID	Number
	Warning	String
Buses.csv	[Optional Index blank header]	Number
	BusID	Number
	Name	String
	Latitude	Number in degrees
	Longitude	Number in degrees
	NominalVoltage	Number
	RealPowerLoad	Number
	ReactivePowerLoad	Number
	Angle	Number
	Voltage	Number
	Frequency	Number
Generator.csv	GeneratorID	Number
	GeneratorName	String
	BusID	Number
	Pmin	Number
	Pmax	Number
	Qmin	Number
	Qmax	Number
	RealPower	Number
	ReactivePower	Number
Interface Lines.csv	InterfaceID	Number
	Line	String
	Coefficient	Number
Interfaces.csv	InterfaceID	Number
	InterfaceName	String
	ForwardLmit	Number
	ReverseLimit	Number
	Flow	Number
Line Fault.csv	LineID	Number
	Description	String

Table 5.2: Data stream file specifications. (*cont.*)

Line Warning.csv	LineID Description	Number String
Lines.csv	LineID Name FromBusID ToBusID Limit ActivePowerFlow ReactivePowerFlow	Number String Number Number Number Number Number
Remedial.csv	RemedialAction Date (M/d/yyyy) Time (h:mm:sstt)	String Date (M/d/yyyy) Time (h:mm:sstt)
System Information.csv	Date (M/d/yyyy) Time (h:mm:sstt)	Date (M/d/yyyy) Time (h:mm:sstt)

6. Application and Discussion

The contribution of the project is implemented on 39-bus system with the cooperation of ERISE lab of Michigan State University (MSU), Los Alamos National Laboratory, Center for Advanced Power Systems of Florida State University (FSU) and LCG Consulting. The project is implemented through the following six steps:

1. Develop the model of 39-bus system on the Real-Time Digital Simulator at Center for Advanced Power Systems of FSU.

2. Streaming real-time data of PMU from a Test system running in real-time on Real-Time Digital Simulator (RTDS) platform. The real-time data streaming is implemented at ERISE lab of MSU.

3. The real-time streaming data is then processed by state estimation tool at ERISE lab of MSU to obtained the necessary data for screening tools.

4. The transient screening and remedial actions tools use the obtained data from state estimation to determine the state of the system in real-time and provide recommended remedial actions. This is implemented at ERISE lab of MSU.

5. The parameters, status of the system and recommended remedial action is sent to the visualization tool at LCG Consulting. These data is also sent to the Real-Time Digital Simulator (RTDS) platform at Center for Advanced Power Systems of FSU.

6.1 Simulation Platform

6.1.1 Real-Time Digital Simulator (RTDS)

RTDS simulation models are typically developed by manually selecting power system and control system components from the RSCAD library of pre-compiled models, and connecting them on the draft page of the development case. When the large power system networks are to be modeled, this can be a very arduous process. To simplify the effort, RTDS has developed a data conversion program as a utility to RSCAD which takes, as input, the load flow description (.raw), dynamic data (.dyr) and sequence data (.seq) employed by the PSS/E software. With very few other command inputs, the conversion program automatically generates the draft (.dft) and runtime (.sib) files for an equivalent RTDS model.

RSCAD comes with a conversion program executable file, “ps2rscad.exe”. With the increasingly use of modeling and simulation by the power industry to analyze network disturbances, FSU-CAPS has used the RSCAD data conversion routine in its program plans for

several large-system modeling efforts. As a result, an effort was under-taken to characterize the scope and accuracy of using ps2rscad.exe as a tool in modeling power system networks comprised of tens to hundreds of buses at the level of detail of the genset (i.e., generator, governor, and exciter). The inputs include the following:

- PSS/E file locations.
- Folder location to receive RSCAD output files.
- The PSS/E version number.
- The desired simulation time step (typically 50 μs).
- The type of load model to use (e.g., constant impedance, constant power, and ZIP).
- The system frequency (60/50 Hz).
- The type of RTDS processor cards available (e.g., GPC, PB5).
- The input bus numbers to include in the model.
- Options about what is converted (i.e., system elements, transmission lines, or generators).

6.1.2 RTDS Results

The first data conversion resulted in a two-subsystem RTDS case. The case is set to run in real-time with a 50 s time-step. The electrical node count for Subsystems 1 and 2 were 51 and 48, respectively. All components of the PSS/E case were included in the RTDS case with the exception of the exciters. The IEEE 39 bus case used in this study employed Simplified Exciter System (SEXS) exciters, which are not represented in the RSCAD exciter library. A note was inserted where the exciters should have been indicating that the proper exciter model was unavailable, and sliders for the field voltage and torque settings were provided instead. The exciter model I in the PSS/e model was replaced by a general model in the RSCAD exciter library, i.e., the IEEE Type 2 exciter. Typical parameter values for this replacement exciter were employed.

No other significant changes were required to the generated RSCAD model. In addition to generating the draft case file, the data conversion routine also creates the following other files that support the user in running the case:

- A runtime, or .sib file with meters to show all bus voltages and generator P, Q, speed, and torque input values.
- A start-up script that unlocks all of the generators at the same time.

The draft case is initialized precisely to the PSS/E loadflow, as evidenced by comparing the bus voltages and angles, and generator P and Q at startup. When the generators are unlocked and go fully dynamic, the bus voltages and power flow through the system drift and settle to new values. However, the system lacks steady-state stability and requires

some tuning of the exciter model, since the parameter settings for this model were adopted from a list of typical values provided by the IEEE. The simulation results from RTDS were confirmed by the results from PSS/E.

6.1.3 Development of PMU Streaming Capability

After simulating the 39-bus system in RTDS, the data is streamed to MSU in real-time. New hardware was acquired for the CAPS RTDS simulator to support the project. The addition of two Giga-Transceiver Network Communication Cards (GTNET), with Phasor Measurement Unit firmware (PMU) increases the total number of GTNET/PMU cards to 4, allowing a total of 96 PMUs in the simulation. The new cards are also synchronized to the existing synchronization card (GTSYNC). All 4 PMU cards which support 24 PMU/card for a total of 96 PMUs in the system have been used to stream data. Successful streaming of PMU data was observed using the PMU connection tester Software.

Figure 6.1 shows the addition and location of PMU units on the NE 39 bus system. The addition of PMU units and their location are given in detail in the excel sheet appended to the report. Each PMU unit requires a unique name with a unique hardware ID code and the output TCP/IP port on which data can be streamed. Each PMU unit can record 12 phasors from each location. In the current simulation, each PMU is set to record two phasors, positive sequence voltage and positive sequence current. The PMU reporting frame rate can be a set from a range of 1–240 Hz. For the simulation, 10 Hz was selected.

Testing of PMU Streaming Using NE 39 Bus system

An open source program, "PMU Connection Tester" was used to test and capture the PMU data streaming from the GTNET PMU cards on RTDS. Two simulation cases were setup to observe data capturing and streaming from PMU cards to the PMU connection tester. A bolted three-phase fault at Bus 13 is used to perform the process. Figure 6.2 shows the streaming data from PMU unit 23 before the fault was applied. Figure 6.3 shows the streaming data from PMU 23 after the fault is applied. Figure 6.4 shows the data stream from PMU 3. The PMU units were successfully added to the IEEE 39 bus system. Streaming data from PMU cards was successfully tested using the "PMU Connection Tester" program.

6.2 Real-Time Data Streaming

A VPN (virtual private networking) connection is established between the MSU and FSU sites to receive real-time data at MSU and send the remedial actions back to the FSU. The screening and remedial action tools read these data in real time frame. The real-time data is dropped in MSU server at frequency of 10 samples per second (this can go up to 60). Once these data are received, the screening and remedial action tools update the status of the system and determine a list of possible harmful contingencies and current contingency(ies) if there is any.

The test to stream data for a specific contingency list for the IEEE 39-bus test system was implemented successfully. The contingency list is as follows:

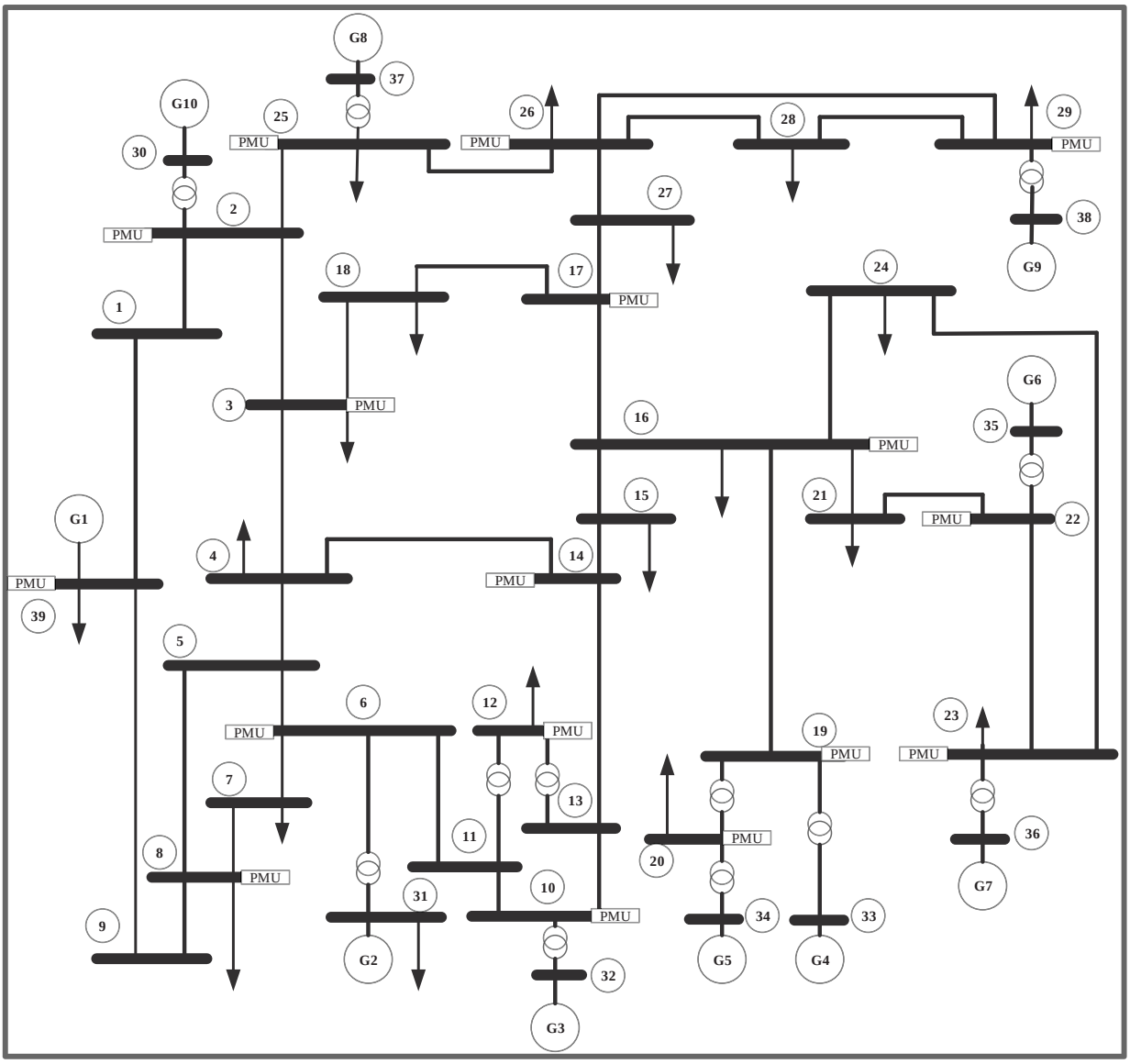

Figure 6.1: NE 39-bus system with PMUs.

1. A three phase fault at bus 16; line 16-19 opened after 0.1 seconds.
2. A three phase fault at bus 1; line 1-2 opened after 0.1 seconds.
3. A three phase fault at bus 26; line 26-27 opened after 0.1 seconds.
4. A three phase fault at bus 16; line 16-17 opened after 0.1 seconds.

The connection between MSU and FSU was made through the CISCO Systems VPN Client.

The measurements of the frequency, voltages and currents at bus # 1 is shown in Fig. 6.5

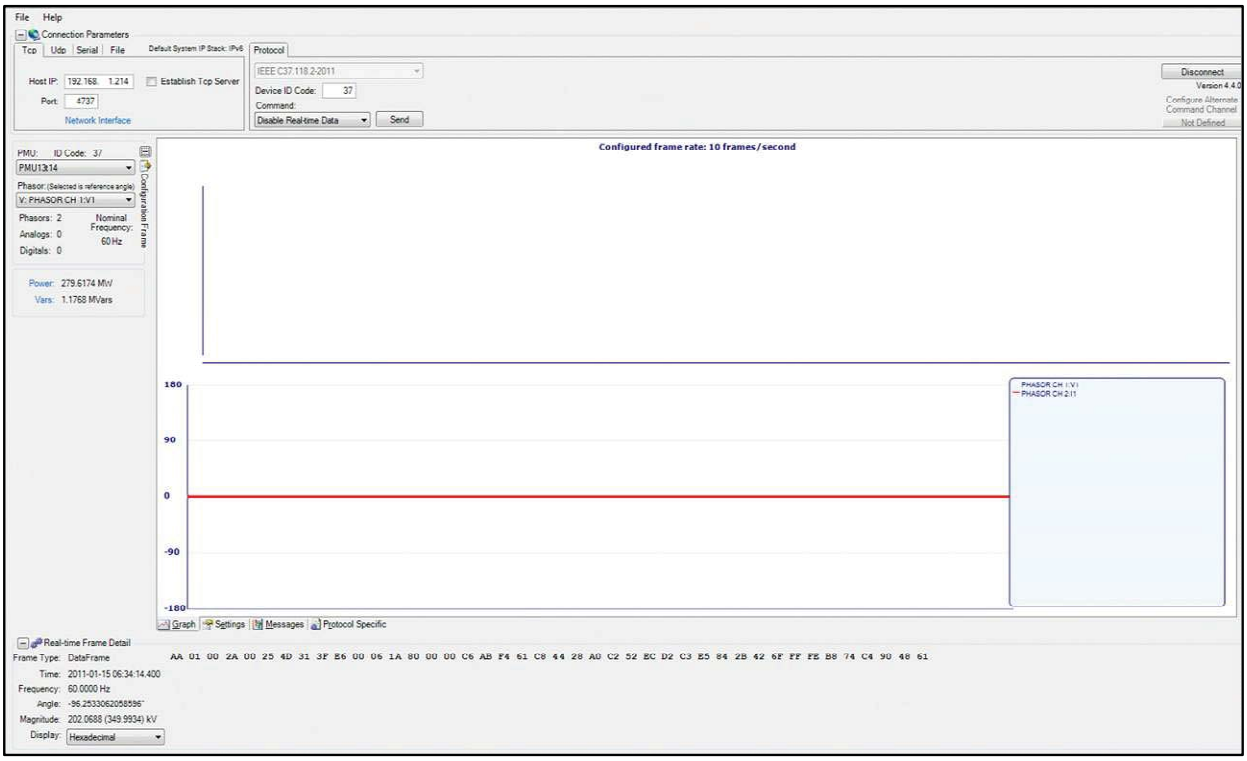

Figure 6.2: Data stream from PMU unit 23 before three-phase fault at bus 13.

6.3 PMU and State Estimation

The NE 39-bus system, needs a total of 17 PMUs to guarantee total system observability under $N-1$ contingencies [54, 55]. Therefore, 17 PMUs were used for estimating NE 39-bus system. The mean square error (MSE) was used to measure the proficiency of the method. The simulation was done with the assumption of noiseless measurement data and with an addition of 10% noise to all measurements. The results are shown in Tables 6.1.

$$MSEm = \sqrt{\frac{1}{N}\sum(\hat{v}_i - v_i^{actual})} \tag{6.1}$$

$$MSEa = \sqrt{\frac{1}{N}\sum(\hat{\theta}_i - \theta_i^{actual})} \tag{6.2}$$

Table 6.1: NE 39-bus system state estimation using Kalman and WLS.

Approach	Magnitude MSEm (noiseless)	Angle MSEa (noiseless)	MSEm (with noise)	Angle MSEa with noise (with noise)
WLS	4.956×10^{-6}	1.3×10^{-4}	8.8×10^{-3}	4.9×10^{-2}
KALMAN	6.76×10^{-6}	5.699×10^{-4}	8.9×10^{-3}	4.09×10^{-2}

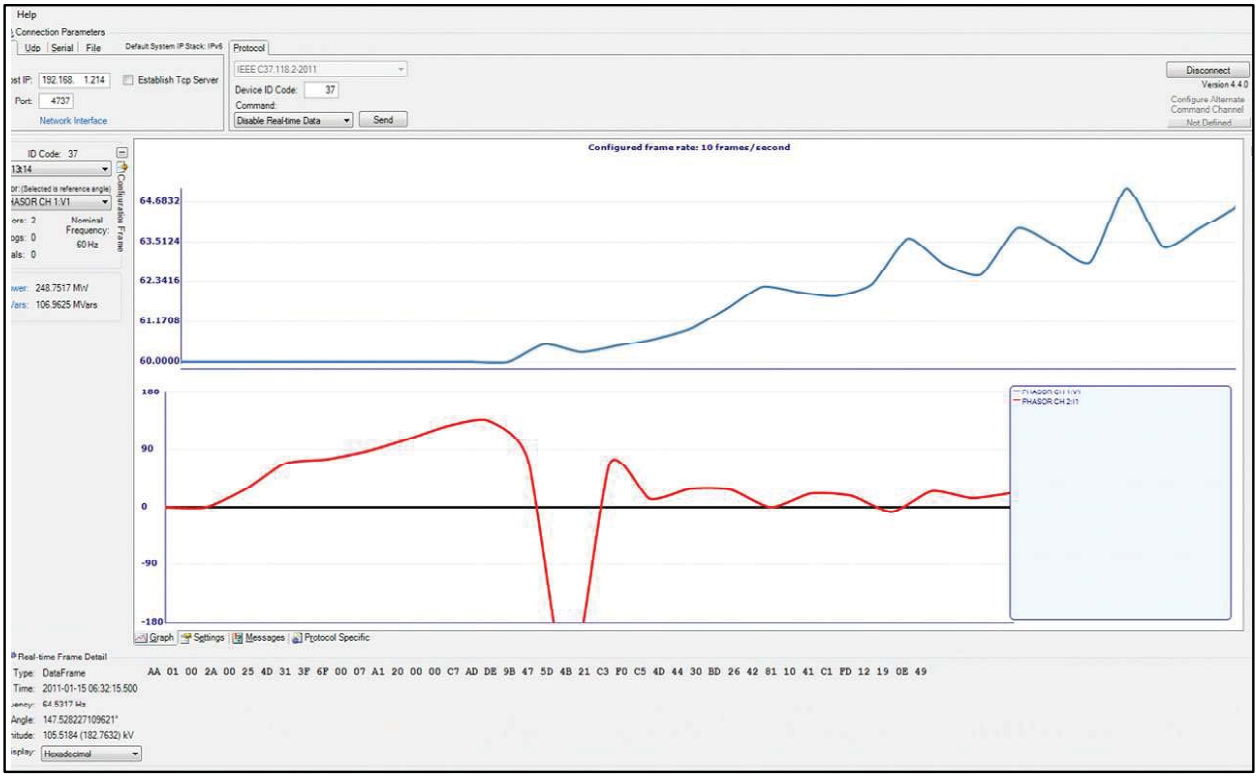

Figure 6.3: Data stream from PMU unit 23 after three-phase fault at bus 13.

6.4 Transient Stability Analysis

The L-RAS tool has been demonstrated on the SCE and NE 39 bus systems. Tables 6.2, 6.3, 6.4, and Tables 6.5 and 6.6 show the controlling UEPs of the contingencies for NE 39-bus system.

6.5 Remedial Actions

After screening, the energy margin of contingencies is calculated to determine the appropriate remedial actions. The energy margin of contingencies is shown in Tables 6.7 and 6.8. The preventive action results are presented in Table 6.9. The corrective actions are presented in Table 6.10. The corrective actions are implemented as a step of 0.01 *pu*.

6.6 Sending Remedial Action Signals to RTDS

After the system status and recommended remedial actions are known, the visualization tool can show the status of the system and recommended remedial actions. If the users chose to implement the remedial actions, the signal of remedial actions is sent back to RTDS. This section presents the approach to send the remedial action signal from MSU to FSU/CAPS.

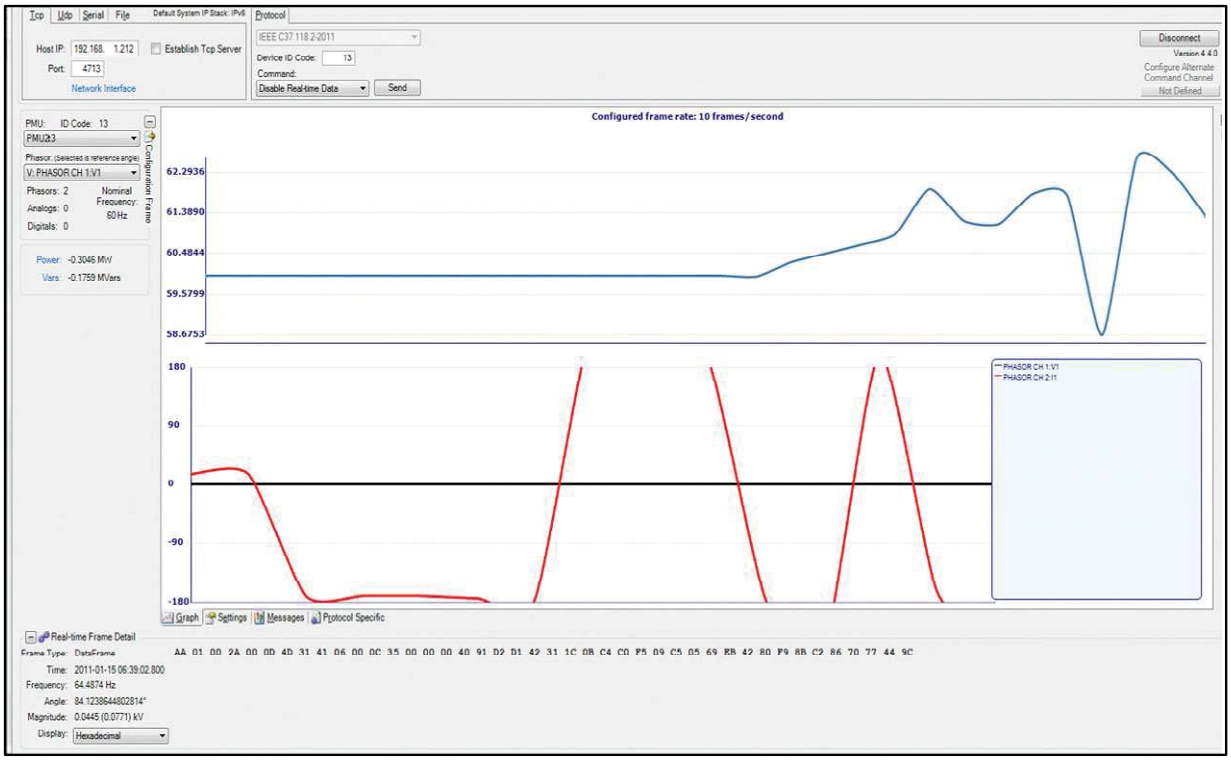

Figure 6.4: Data stream from PMU unit 3 after three-phase fault at bus 13.

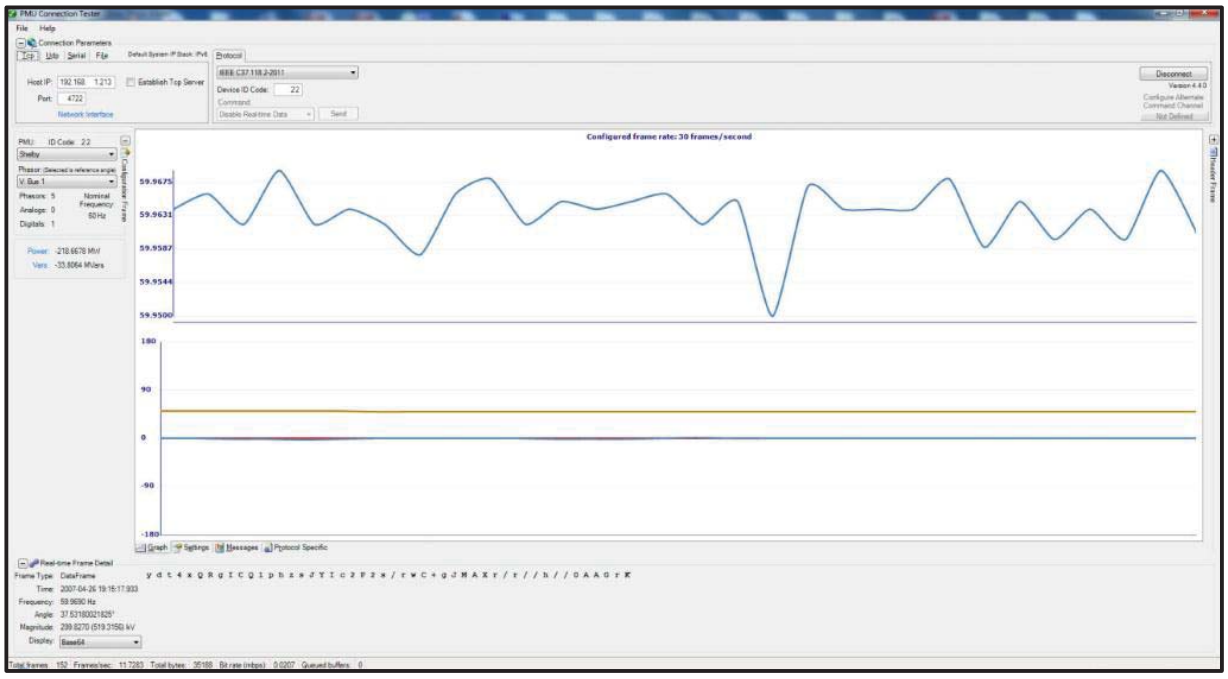

Figure 6.5: Data streaming from FSU to MSU through the PMU connection tester software.

Table 6.2: Simulation results of the NE 39-bus system.

Faulted Bus	Tripped Line		Controlling UEPs (δ_1,δ_2, $\cdots$, δ_{10}) (Rad)				
	From	To					
1	1	2	−1.3013	2.7573	2.6174	2.2003	2.2820
			2.2171	2.2400	2.2316	2.3452	1.8976
2	1	2	−1.3013	2.7573	2.6174	2.2003	2.2820
			2.2171	2.2400	2.2316	2.3452	1.8976
1	1	39	−1.3214	2.7956	2.6579	2.2356	2.3163
			2.2522	2.2748	2.2653	2.3758	1.9345
39	1	39	−1.3214	2.7956	2.6579	2.2356	2.3163
			2.2522	2.2748	2.2653	2.3758	1.9345
2	2	3	−0.1708	−0.1564	−0.1575	−0.1872	−0.1021
			−0.1707	−0.1474	2.5571	1.8152	−0.2649
3	2	3	−0.9547	2.2214	2.1303	1.8522	1.9678
			1.8677	1.8953	0.7979	2.7504	0.0082
2	2	25	−0.9795	2.5886	2.2507	1.7183	1.8343
			1.7308	1.7590	1.8709	2.0038	0.3010
25	2	25	−0.9394	1.3543	1.4139	1.7046	1.8381
			1.7146	1.7453	2.7322	3.0795	0.0744
3	3	4	−0.9903	2.0047	1.9228	1.6103	1.7240
			1.6247	1.6525	1.4133	3.1593	0.7425
4	3	4	−0.0259	2.3553	0.1709	−0.3027	−0.2265
			−0.2867	−0.2647	−0.2244	−0.1602	−0.5248
3	3	18	−0.0088	2.3123	0.0136	−0.3647	−0.2897
			−0.3477	−0.3256	−0.1522	−0.1377	−0.4535
18	3	18	−0.0092	2.3121	0.0146	−0.3639	−0.2894
			−0.3467	−0.3248	−0.1515	−0.1371	−0.4528
4	4	5	0.0104	2.3336	0.0366	−0.3865	−0.3129
			−0.3705	−0.3490	−0.2470	−0.1928	−0.5536
5	4	5	0.0104	2.3331	0.0367	−0.3865	−0.3123
			−0.3704	−0.3489	−0.2471	−0.1928	−0.5540
4	4	14	−0.0288	2.3148	0.0147	−0.2831	−0.2086
			−0.2665	−0.2448	−0.1601	−0.0940	−0.4726

In order to make an efficient communication, a common language is required. The communication protocol is utilized as the common language to accomplish this goal. In this project, the TCP/IP protocol is applied, since the TCP/IP protocol suite allows computers of all sizes, from many different computer vendors, running totally different operating systems, to communicate with each other [60]. Besides, it is a widely used open system and many of its implementations are publicly available. Server and client are two distinct categories of socket network applications. There are two types of servers, iterative or concurrent. In general, Transmission Control Protocol (TCP) servers are concurrent while User Datagram

Table 6.3: Simulation results of the NE 39-bus system. (*cont.*)

Faulted Bus	Tripped Line		Controlling UEPs ($\delta_1, \delta_2, \cdots, \delta_{10}$) (Rad)				
	From	To					
5	5	6	−0.0249	2.3266	0.0596	−0.3020	−0.2256
			−0.2854	−0.2634	−0.1778	−0.1147	−0.4887
6	5	6	−0.0246	2.3262	0.0584	−0.3027	−0.2275
			−0.2859	−0.2639	−0.1780	−0.1150	−0.4886
5	5	8	−0.9760	3.0732	2.3373	1.5884	1.7001
			1.6037	1.6310	1.3118	1.6826	0.7805
8	5	8	−0.9767	3.0736	2.3388	1.5901	1.7019
			1.6049	1.6320	1.3131	1.6833	0.7821
6	6	7	−0.9641	3.0666	2.3539	1.5686	1.6830
			1.5821	1.6094	1.2692	1.6525	0.7344
6	6	11	−0.3541	2.2697	2.3965	0.1645	0.2617
			0.1794	0.2048	0.0853	0.2625	−0.2809
11	6	11	−0.3552	2.2709	2.3964	0.1669	0.2651
			0.1820	0.2073	0.0875	0.2649	−0.2796
7	7	8	−0.9740	3.0725	2.3631	1.5862	1.7011
			1.6016	1.6285	1.2933	1.6752	0.7558
8	7	8	−0.9745	3.0742	2.3626	1.5870	1.7010
			1.6021	1.6291	1.2957	1.6769	0.7576
8	8	9	−1.5375	2.6757	2.6813	2.6223	2.6982
			2.6378	2.6602	2.9641	2.9709	2.6185
9	8	9	−1.5419	2.6840	2.6888	2.6295	2.7047
			2.6457	2.6683	2.9722	2.9779	2.6280
10	10	11	−0.3500	2.2740	2.3853	0.1535	0.2506
			0.1686	0.1937	0.0803	0.2561	−0.2853
11	10	11	−0.3492	2.2731	2.3849	0.1520	0.2494
			0.1663	0.1914	0.0802	0.2537	−0.2863
10	10	13	−0.0579	0.1983	2.3331	−0.3078	−0.2302
			−0.2911	−0.2690	−0.1755	−0.1075	−0.4907
13	10	13	−0.0579	0.1983	2.3331	−0.3080	−0.2301
			−0.2911	−0.2690	−0.1756	−0.1076	−0.4906

Protocol (UDP) servers are iterative. In this project, MSU is the client side which should be able to send one set of remedial action signals to FSU/CAPS every 10 seconds. FSU/CAPS is set as the server side, which should receive the real-time data from MSU and then adjust the RTDS according to the signals.

Table 6.4: Simulation results of the NE 39-bus system. (*cont.*)

Faulted Bus	Tripped Line		Controlling UEPs ($\delta_1, \delta_2, \cdots, \delta_{10}$) (Rad)				
	From	To					
13	13	14	−0.0466	0.2460	2.3384	−0.3482	−0.2729
			−0.3315	−0.3098	−0.1991	−0.1391	−0.5114
14	13	14	−0.0469	0.2471	2.3388	−0.3479	−0.2725
			−0.3311	−0.3094	−0.1983	−0.1381	−0.5111
14	14	15	−0.0362	0.3627	2.3747	−0.4380	−0.3647
			−0.4227	−0.4009	−0.1850	−0.1503	−0.4976
15	14	15	−0.0358	0.3632	2.3745	−0.4395	−0.3673
			−0.4234	−0.4018	−0.1854	−0.1518	−0.4977
15	15	16	−0.0553	0.3353	2.3510	−0.3634	−0.2951
			−0.3464	−0.3254	−0.1632	−0.1204	−0.4723
16	15	16	−0.0553	0.3350	2.3510	−0.3631	−0.2959
			−0.3464	−0.3253	−0.1628	−0.1196	−0.4724
16	16	17	−0.7088	0.8479	1.0814	2.5514	2.7047
			2.5602	2.5930	−0.0137	0.1799	−0.3980
17	16	17	−1.0535	2.0605	1.9641	1.6260	1.7137
			1.6418	1.6648	1.9512	3.0368	1.1827
16	16	21	−1.0917	2.3978	2.2595	1.8758	1.9829
			1.9451	1.9609	1.7788	2.0729	1.2596
21	16	21	−0.8805	0.9763	1.0658	1.7841	1.9895
			3.0974	3.1100	0.8177	1.4478	0.2388
16	16	24	−1.1011	2.4690	2.3185	1.8922	1.9981
			1.8486	1.8566	1.8395	2.1144	1.3259
24	16	24	−1.1012	2.4694	2.3166	1.8921	1.9970
			1.8489	1.8574	1.8411	2.1138	1.3274
17	17	18	−0.0130	2.3092	0.0103	−0.3406	−0.2680
			−0.3232	−0.3021	−0.1601	−0.1295	−0.4651
18	17	18	−0.0133	2.3098	0.0112	−0.3399	−0.2670
			−0.3230	−0.3022	−0.1599	−0.1293	−0.4650
17	17	27	−1.0581	1.8905	1.8381	1.6533	1.7570
			1.6678	1.6943	1.9580	3.2930	1.1670

6.6.1 Layering of TCP/IP Protocol Suite

The layering is an essential concept of networking protocol which is developed for different functions of the network. The function of each layer in different network models may not be the same. A protocol suite, such as TCP/IP, is the combination of different protocols at various layers [60]. Figure 6.6 shows the 4-layers model of the TCP/IP suite. They are the link layer, the network layer, the transport layer and the application layer. Each layer has its own responsibility and functions.

Table 6.5: Simulation results of the NE 39-bus system. (*cont.*)

Faulted Bus	Tripped Line		Controlling UEPs ($\delta_1, \delta_2, \cdots, \delta_{10}$) (Rad)				
	From	To					
27	17	27	−1.0581	1.8898	1.8383	1.6539	1.7569
			1.6681	1.6937	1.9585	3.2937	1.1674
21	21	22	−0.2880	0.0015	0.0240	0.2125	0.3335
			2.2287	2.2150	0.0060	0.2036	−0.3535
22	21	22	−0.2883	0.0018	0.0245	0.2132	0.3355
			2.2291	2.2156	0.0061	0.2035	−0.3531
22	22	23	−0.8594	1.0292	1.1177	1.7906	1.9880
			3.5067	1.8413	0.8728	1.4874	0.2959
23	22	23	−0.9547	1.5127	1.5471	1.7953	1.9505
			1.8049	3.7077	1.1846	1.7150	0.6060
23	23	24	−1.0922	2.3543	2.2297	1.8825	1.9884
			1.9630	2.0057	1.7841	2.0708	1.2696
24	23	24	−1.0924	2.3530	2.2287	1.8835	1.9886
			1.9639	2.0060	1.7846	2.0732	1.2702
25	25	26	−0.2374	−0.0099	0.0011	0.0147	0.1045
			0.0315	0.0556	2.5252	1.9525	−0.3682
26	25	26	−1.0151	1.8740	1.8448	1.8133	1.9336
			1.8280	1.8566	1.1738	3.3018	0.6558
26	26	27	−1.0152	1.8744	1.8450	1.8131	1.9325
			1.8280	1.8567	1.1736	3.3032	0.6555
27	26	27	−1.0149	1.8739	1.8446	1.8133	1.9335
			1.8276	1.8562	1.1731	3.3008	0.6552
26	26	28	−1.0552	1.9587	1.9031	1.7331	1.8425
			1.7480	1.7750	1.6767	3.2208	1.0262
28	26	28	−0.0107	−0.1665	−0.1784	−0.2857	−0.2141
			−0.2690	−0.2473	−0.0578	1.9207	−0.4394
26	26	29	−1.0566	1.9793	1.9200	1.7408	1.8489
			1.7568	1.7833	1.6866	3.1476	1.0467
29	26	29	−0.0072	−0.1665	−0.1787	−0.2873	−0.2158
			−0.2703	−0.2489	−0.0601	1.8780	−0.4404

1. The link layer, which is also called the data-link layer or network interface layer. It is the lowest component layer of the Internet Protocols (IP). It usually corresponds to the hardware, including the device driver in the operating system and the corresponding network interface card in the computer.

2. The network layer or the internet layer manages the movement of packets around the network. It provides a basic service of packet delivery from one host to another host. For example, IP (Internet Protocol), ICMP (Internet Control Message Protocol), and IGMP (Internet Group Management Protocol) provide the network layer in the TCP/IP protocol

Table 6.6: Simulation results of the NE 39-bus system. (*cont.*)

Faulted Bus	Tripped Line		Controlling UEPs ($\delta_1, \delta_2, \cdots, \delta_{10}$) (Rad)				
	From	To					
28	28	29	0.0049	−0.1790	−0.1935	−0.3092	−0.2374
			−0.2927	−0.2706	−0.0834	1.8433	−0.4606
29	28	29	0.0050	−0.1790	−0.1936	−0.3096	−0.2376
			−0.2929	−0.2707	−0.0833	1.8432	−0.4607
12	12	11	−1.1069	2.4035	2.2721	1.9044	2.0060
			1.9187	1.9442	1.8514	2.1113	1.3512
11	12	11	−0.3383	2.2720	2.3699	0.1207	0.2167
			0.1355	0.1601	0.0691	0.2364	−0.2951
12	12	13	−1.1075	2.4046	2.2707	1.9055	2.0070
			1.9195	1.9453	1.8535	2.1129	1.3531
13	12	13	−0.3381	2.2714	2.3706	0.1201	0.2155
			0.1347	0.1596	0.0684	0.2359	−0.2945

Table 6.7: The energy margin of contingencies for NE 39-bus system.

Faulted Bus	Tripped Line		Energy margin	Status
	From	To		
1	1	2	1.132942	Stable
2	1	2	−0.748455	Unstable
1	1	39	1.575947	Stable
1	2	3	4.209352	Stable
3	2	3	2.748032	Stable
2	2	25	−1.009539	Unstable
25	2	25	−1.706865	Unstable
3	3	4	3.561293	Stable
4	3	4	4.106192	Stable
3	3	18	4.275501	Stable
18	3	18	4.124130	Stable
5	4	5	5.267969	Stable
4	4	14	5.421871	Stable
14	4	14	5.161829	Stable
5	5	6	3.980721	Stable
6	5	6	4.062622	Stable
6	6	11	4.315691	Stable
9	8	9	2.966698	Stable
9	9	39	3.597103	Stable
39	9	39	3.442142	Stable

Table 6.8: The energy margin of contingencies for NE 39-bus system. (*cont.*)

Faulted Bus	Tripped Line		Energy margin	Status
	From	To		
14	14	15	−30.16628	Unstable
17	16	17	2.478556	Stable
16	16	21	2.777214	Stable
21	16	21	3.475832	Stable
16	16	24	4.649857	Stable
24	16	24	4.696455	Stable
17	17	18	3.221983	Stable
18	17	18	3.775555	Stable
17	17	27	3.562017	Stable
27	17	27	−0.663641	Unstable
24	23	24	3.267786	Stable
25	25	26	8.190344	Stable
26	25	26	−0.860172	Unstable
26	26	27	3.734009	Stable
27	26	27	−0.621422	Unstable
26	26	28	−1.375554	Unstable
28	26	28	−0.434653	Unstable
26	26	29	−1.669645	Unstable
29	26	29	−40.76310	Unstable
28	28	29	−0.956303	Unstable
29	28	29	−1.264503	Unstable
12	12	11	6.189329	Stable
12	12	13	6.201702	Stable

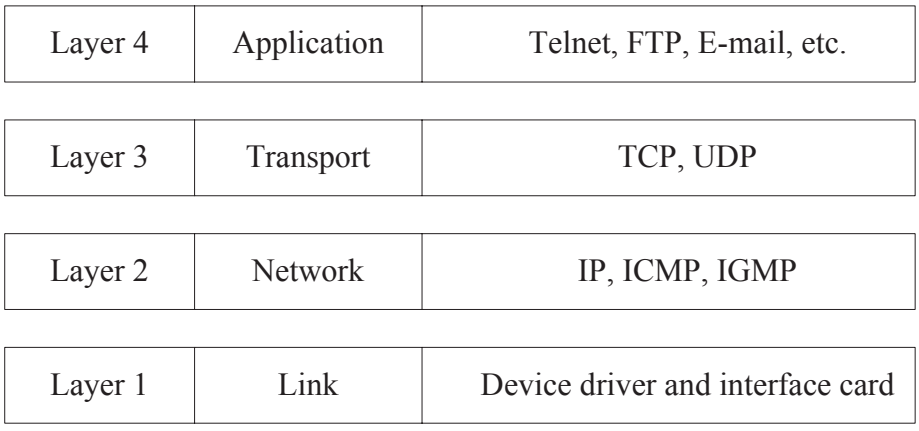

Figure 6.6: The four layers of the TCP/IP protocol suite.

Table 6.9: Preventive actions based on sensitivity calculation.

Faulted Bus	Tripped Line From	Tripped Line To	Energy margin	ΔP_{m1} ΔP_{m6}	ΔP_{m2} ΔP_{m7}	ΔP_{m3} ΔP_{m8}	ΔP_{m4} ΔP_{m9}	ΔP_{m5} ΔP_{m10}
2	1	2	−0.748455	−0.1781 0.0259	−0.0121 0.0229	0.0055 0.0282	0.0195 0.0300	0.0266 0.0315
2	2	25	−1.009539	0.0536 −0.0627	−0.0025 0.0565	0.0068 −0.0224	−0.0063 −0.0235	0.0084 −0.0078
25	2	25	−1.706865	0.0295 −0.0659	−0.0013 0.1034	0.0108 −0.0394	−0.0059 −0.0417	0.0250 −0.0144
14	14	15	−30.16628	Not available				
17	17	27	−0.663641	0.2361 −0.0228	0.0052 −0.0385	−0.0249 −0.0374	−0.0196 −0.0479	−0.0220 −0.0282
26	25	26	−0.8601723	−0.3185 0.3711	0.0616 −0.2601	−0.1815 −0.0940	0.2281 −1.0979	0.2384 0.4157
27	26	27	−0.6214218	0.1375 −0.0154	−0.0036 −0.0196	−0.0098 −0.0184	−0.0129 −0.0237	−0.0156 −0.0185
26	26	28	−1.375554	0.6691 −0.0528	−0.0450 −0.0229	−0.0530 −0.0873	−0.0802 −0.1921	−0.0508 −0.0850
28	26	28	−0.434653	0.0592 −0.0082	−0.0026 0.0004	−0.0031 −0.0047	−0.0044 −0.0088	−0.0232 −0.0047
26	26	29	−1.669645	−0.3382 0.0449	0.0250 0.0063	0.0573 0.0410	0.0399 0.0345	0.0423 0.0471
29	26	29	−40.76310	Not available				
28	28	29	−0.9563029	−0.0243 −0.0011	−0.0004 0.0305	−0.0004 −0.0017	0.0003 −0.0032	0.0018 −0.0013
29	28	29	−1.264503	0.4545 −0.1145	−0.0275 −0.0108	−0.0360 −0.0551	−0.0799 −0.1299	0.0478 −0.0485

suite.

3. The transport layer is used to exchange data between two hosts. The two types of transport protocols are TCP (Transmission Control Protocol) and UDP (User Datagram Protocol).

In this project, the TCP is applied, which is able to provide reliable data flow between server and client. Although UDP provides a much simpler service to the application layer. It just sends packets of data called datagrams from one host to the other, but there is no guarantee that the datagrams reach the other end [60].

4. The application layer handles the details of the particular application. There are many common TCP/IP applications that almost every implementation provides [60].

Table 6.10: Corrective actions based on sensitivity calculation.

Faulted Bus	Tripped Line		Energy margin	Corrective action		
	From	To		Type	Bus	$\Delta P_{corrective}$
2	1	2	−0.748455	Load shedding	12	0.04
2	2	25	−1.009539	Generation tripping	39	0.11
25	2	25	−1.706865	Generation tripping	31	0.18
14	14	15	−30.16628	Generation tripping	30	1.06
17	17	27	−0.663641	Resistance application	15	0.06
26	25	26	−0.860172	Generation tripping	38	0.14
27	26	27	−0.621422	Generation tripping	33	0.10
26	26	28	−1.375554	Resistance application	15	0.06
28	26	28	−0.434653	Generation tripping	32	0.03
26	26	29	−1.669645	Generation tripping	33	0.13
29	26	29	−40.76310	Generation tripping	33	0.51
28	28	29	−0.956303	Generation tripping	35	0.05
29	28	29	−1.264503	Generation tripping	37	0.23

6.6.2 The Windows Sockets API

The Windows Sockets application programming interface (API) is commonly known as WinSock which enables programmers to create advanced Internet, intranet, and other network-capable applications to transmit application data across the wire, independent of the network protocol being used. It defines a standard interface between a Windows TCP/IP client application and the underlying TCP/IP protocol stack. Using Winsock, we can have the access to advanced Microsoft Windows networking capabilities. It follows the Windows Open System Architecture (WOSA) model; it defines a standard service provider interface (SPI) between the application programming interface (API), with its exported functions and the protocol stacks [61]. The sockets paradigm is based on the Berkeley sockets API model used in Berkeley Software Distribution (BSD)for communications between programs.

Server and client are two distinct types of socket network applications. They have different behaviors and the process of creating them is different, although few steps are the same for both client and server applications. Figure 6.7 shows the general model for creating a streaming TCP/IP Server and Client.

6.6.3 Data Communication between L-RAS Site and RTDS

The client executive file TCPClient.exe is implemented by C++ with WinSock2. In general, the remedial action signals are saved in a file in binary format written by our Fortran program. The signals include generator setting points, load setting points, from/to bus numbers of the line which should be tripped. After creating the remedial actions file, the TCPClient.exe is run to connect to the RTDS TCP server on the GTNET card in FSU/CAPS. (A VPN connection needs to be established before starting the TCP client.)

Once the TCP server is turned on at RTDS side and MSU is connected to FSU/CAPS

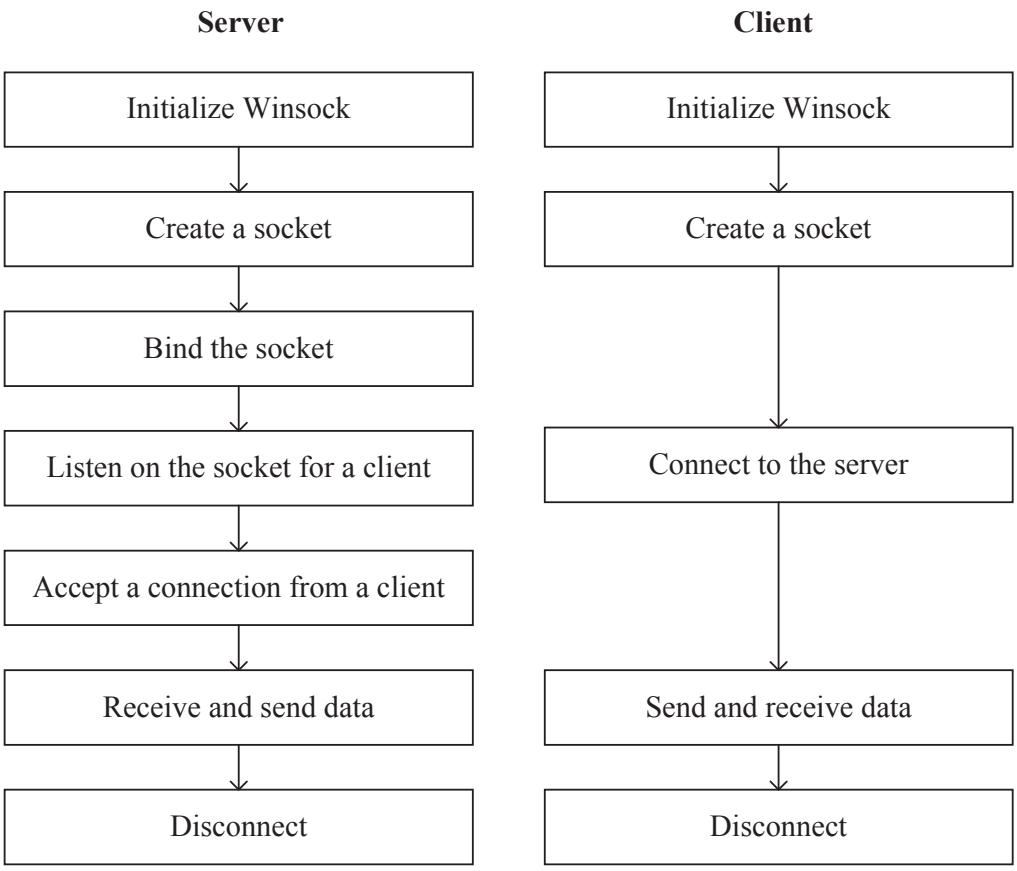

Figure 6.7: The general model for creating a streaming TCP/IP Server and Client.

through VPN, MSU is able to send remedial action signals to RDTS.

6.7 Conclusion

This concludes the description of the development and demonstration of the L-RAS tool that was collaboratively developed by MSU, FSU, LANL and LCG, with support from SCE. As mentioned earlier, due to Critical Energy Infrastructure Information (CEII) restrictions, neither the SCE system, nor demonstrations thereon, are reported here.

The L-RAS represents a significant mathematical innovation toward enabling the understanding of catastrophic failure in power systems and the rapid and correct selection of remedial actions. In conjunction with the RTDS system at FSU-CAPS, this also provides a unique and versatile test-bed for further understanding of these processes, as well as a training tool for system operators.

APPENDICES

A. Real-Time Digital Simulator at FSU

The maximum number of 3-phase buses that can be represented on FSU's RTDS is 286. This is a direct result of its specific hardware configuration, described in Table 1. A 286-node model would require full use of the top eight racks of FSU's 14-RTDS. At present, pss2rscad.exe only allows the user's RTDS configuration to be populated with one type of DSP card in each rack (e.g., 3PC, GPC, PB5 with one processor available to perform the network solution, or PB5 with two processors available to perform a dual-network solution). FSU has requested that RTDS provide greater flexibility in defining the hardware configuration in future program releases.

Table A.1: FSU RTDS hardware configuration.

Rack No.	Fast or Slow Backplane?	No. of GPC Cards	No. of PB5 Cards	No. of Electrical Nodes Possible	No. of 3-phase Buses Possible
1	S	5	0	66	22
2	S	5	0	66	22
3	S	5	0	66	22
4	S	5	0	66	22
5	S	5	0	66	22
6	S	5	0	66	22
7	F	5	0	66	22
8	F	5	0	72	24
9	F	5	0	72	24
10	F	5	0	72	24
11	F	3	2	144	48
12	F	3	2	144	48
13	F	3	2	144	48
14	F	3	2	144	48

Table A.2: Data stream file specifications.

PMU Unit	PMU Name	Hardware ID	TCP/IP Port	IP
1	PMU1t2	11	4711	192.168.1.212
2	PMU1t39	12	4712	192.168.1.212
3	PMU2t3	13	4713	192.168.1.212
4	PMU2t25	14	4714	192.168.1.212
5	PMU2t30	15	4715	192.168.1.212
6	PMU3t4	16	4716	192.168.1.212
7	PMU3t18	17	4717	192.168.1.212
8	PMU4t5	18	4718	192.168.1.212
9	PMU26t27	21	4721	192.168.1.213
10	PMU19t33	22	4722	192.168.1.213
11	PMU20t34	23	4723	192.168.1.213
12	PMU21t22	24	4724	192.168.1.213
13	PMU26t29	25	4725	192.168.1.213
14	PMU6t31	26	4726	192.168.1.213
15	PMU7t8	27	4727	192.168.1.213
16	PMU8t9	28	4728	192.168.1.213
17	PMU9t39	31	4731	192.168.1.214
18	PMU10t11	32	4732	192.168.1.214
19	PMU10t13	33	4733	192.168.1.214
20	PMU10t32	34	4734	192.168.1.214
21	PMU11t12	35	4735	192.168.1.214
22	PMU12t13	36	4736	192.168.1.214
23	PMU13t14	37	4737	192.168.1.214
24	PMU14t15	38	4738	192.168.1.214
25	PMU15t16	41	4741	192.168.1.215
26	PMU16t17	42	4742	192.168.1.215
27	PMU16t19	43	4743	192.168.1.215
28	PMU16t21	44	4744	192.168.1.215
29	PMU16t24	45	4745	192.168.1.215
30	PMU17t18	46	4746	192.168.1.215
31	PMU17t27	47	4747	192.168.1.215
32	PMU19t20	48	4748	192.168.1.215

BIBLIOGRAPHY

BIBLIOGRAPHY

[1] H. Chiang, *Direct Methods for Stability Analysis of Electric Power Systems: Theoretical Foundation, BCU Methodologies, and Applications*. John Wiley & Sons, 2011.

[2] H. Chiang, C. Wang, and H. Li, "Development of BCU Classifiers for On-Line Dynamic Contingency Screening of Electric Power Systems," *IEEE Trans. Power Syst.*, vol. 14, no. 2, pp. 660–666, May 1999.

[3] H. Chiang, C. Chu, and G. Cauley, "Direct Stability Analysis of Electric Power Systems using Energy Functions: Theory, Applications, and Perspective," *Proceedings of the IEEE*, vol. 83, no. 11, pp. 1497–1529, Nov. 1995.

[4] M. Benidris, N. Cai, and J. Mitra, "A fast transient stability screening and ranking tool," in *Power Systems Computation Conference (PSCC)*, Aug. 2014, pp. 1–7.

[5] J. Mitra, M. Benidris, and N. Cai, "Tool Employing Homotopy-Based Approaches in Finding the Controlling Unstable Equilibrium Points in the Electric Power Grid," Patent 20 160 041 232, February, 2016. [Online]. Available: http://www.freepatentsonline.com/y2016/0041232.html

[6] D. Sobajic and Y. Pao, "Artificial Neural-net based Dynamic Security Assessment for Electric Power Systems," *IEEE Trans. Power Syst.*, vol. 4, no. 1, pp. 220–228, Feb. 1989.

[7] V. Brandwajn, A. Kumar, A. Ipakchi, A. Bose, and S. Kuo, "Severity Indices for Contingency Screening in Dynamic Security Assessment," in *Proc. of the IEEE Power Eng. Soc. Summer Meeting*, Denver, CO, USA, July 28 – Aug. 2 1996.

[8] H. Hakimmashhadi and G. Heydt, "Fast Transient Stability Assessment," *IEEE Trans. Power App. Syst.*, vol. PAS–102, pp. 3816–3824, Dec. 1983.

[9] Y. Akimoto, H. Tanaka, J. Yoshizawa, D. Klapper, and K. Price, "Transient Stability Expert Systems," *IEEE Trans. Power Syst.*, vol. 4, no. 1, pp. 312–320, Jan. 1989.

[10] L. Wehenkel, M. Pavella, E. Euxibie, and B. Heilbronn, "Decision Tree based Transient Stability Method a Case Study," *IEEE Trans. Power Syst.*, vol. 9, no. 1, pp. 459–469, Feb. 1994.

[11] "Power System Dynamic Security Analysis Using Artificial Intelligence Systems: Phase 1–Feasibility Evaluation," Tech. Rep., EPRI TR-103607 Project 3103-02, Final Report, Apr. 1994.

[12] Y. Mansour, E. Vaahedi, A. Chang, B. Corns, J. Tamby, and M. El-Sharkawi, "Large Scale Dynamic Security Screening and Ranking using Neural Networks," *IEEE Trans. Power Syst.*, vol. 12, no. 2, pp. 954–960, May 1997.

[13] L. Moulin, A. Alves da Silva, M. El-Sharkawi, and R. Marks II, "Support Vector Machines for Transient Stability Analysis of Large-Scale Power Systems," *IEEE Trans. Power Syst.*, vol. 19, no. 2, pp. 818–825, May 2004.

[14] A. Gavoyiannis, D. Vogiatzis, D. Georgiadis, and N. Hatziargyriou, "Combined support vector classifiers using fuzzy clustering for dynamic security assessment," in *Proc. of the IEEE Power Eng. Soc. Summer Meeting*, vol. 2, Vancouver, BC, 2001.

[15] L. Moulin, A. Alves da Silva, M. El-Sharkawi, R. Marks *et al.*, "Support Vector and Multilayer Perceptron Neural Networks Applied to Power Systems Transient Stability Analysis with Input Dimensionality Reduction," in *Proc. of the IEEE Power Eng. Soc. Summer Meeting*, vol. 3. IEEE, 2002, pp. 1308–1313.

[16] I. Kassabalidis, M. El-Sharkawi, R. Marks II, L. Moulin, and A. Alves da Silva, "Dynamic Security Border Identification using Enhanced Particle Swarm Optimization," *IEEE Trans. Power Syst.*, vol. 17, no. 3, pp. 723–729, Aug. 2002.

[17] Y. Mansour, E. Vaahedi, and M. El-Sharkawi, "Dynamic Security Contingency Screening and Ranking using Neural Networks," *IEEE Trans. Neural Netw.*, vol. 8, no. 4, pp. 942–950, Jul. 1997.

[18] I. Kamwa, R. Grondin, and L. Loud, "Time-Varying Contingency Screening for Dynamic Security Assessment using Intelligent-Systems Techniques," *IEEE Trans. Power Syst.*, vol. 16, no. 3, pp. 526–536, Aug. 2001.

[19] Y. Park, G. Kim, H. Cho, and K. Lee, "A New Algorithm for Kohonen Layer Learning with Application to Power System Stability Analysis," *IEEE Trans. Power Syst.*, vol. 27, no. 6, pp. 1030–1034, Dec. 1997.

[20] K. Chan, A. Edwards, R. Dunn, and A. Daniels, "On-Line Dynamic Security Contingency Screening using Artificial Neural Networks," *IEE Proc. Generat. Transm. Distrib.*, vol. 147, no. 6, pp. 367–372, Nov. 2000.

[21] V. Brandwajn, A. Kumar, A. Ipakchi, A. Bose, and S. Kuo, "Severity Indices for Contingency Screening in Dynamic Security Assessment," *IEEE Trans. Power Syst.*, vol. 12, no. 3, pp. 1136–1142, Aug. 1997.

[22] "Analytical Methods for Contingency Selection and Ranking for Dynamic Security Analysis," Tech. Rep., EPRI TR-104352, Project 3103-03, Final Report, Siemens Energy & Automation Inc., Sept. 1994.

[23] V. Chadalavada, V. Vittal, G. Ejebe, G. Irissari, J. Tong, G. Pieper, and M. McMullen, "An On-Line Contingency Filtering Scheme for Dynamic Security Assessment," *IEEE Trans. Power Syst.*, vol. 12, no. 1, pp. 153–161, Feb. 1997.

[24] H. Chiang, H. Li, J. Tong, and Y. Tada, *High Performance Computing in Power and Energy Systems*. Springer Heidelberg New York Dordrecht, London, 2013, ch. On-Line Transient Stability Screening of a Practical 14,500-Bus Power System: Methodology and Evaluations, pp. 335–358.

[25] S. Kim, Y. Tada, and S. Hur, "Transient Contingency Screening of Large Power Systems using Tepco-BCU Classifier," in *Proc. of the International Conference on Electrical Engineering, ICEE*, Shenyang, China, 2009.

[26] D. Ernst, D. Ruiz-Vega, M. Pavella, P. Hirsch, and D. Sobajic, "A Unified Approach to Transient Stability Contingency Filtering, Ranking and Assessment," *IEEE Trans. Power Syst.*, vol. 16, no. 3, pp. 435–443, Aug. 2001.

[27] Y. Mansour, E. Vaahedi, A. Chang, B. Corns, B. Garrett, K. Demaree, T. Athay, and K. Cheung, "B. C. Hydro's On-line Transient Stability Assessment (TSA): Model Development, Analysis and Post-processing," *IEEE Trans. Power Syst.*, vol. 10, no. 1, pp. 241–253, Feb. 1995.

[28] T. Athay, R. Podmore, and S. Virmani, "A Practical Method for the Direct Analysis of Transient Stability," *IEEE Trans. Power App. Syst.*, vol. PAS-98, no. 2, pp. 573–584, Mar. 1979.

[29] A. Fouad and S. Stanton, "Transient Stability of a Multi-Machine Power System Part I: Investigation of System Trajectories," *IEEE Trans. Power App. Syst.*, vol. PAS-100, no. 7, pp. 3408–3416, July 1981.

[30] P. Varaiya, F. Wu, and R. Chen, "Direct Methods for Transient Stability Analysis of Power Systems: Recent Results," *Proceedings of the IEEE*, vol. 73, no. 12, pp. 1703–1715, Dec. 1985.

[31] H. Chiang, F. Wu, and P. Varaiya, "Foundations of Direct Methods for Power System Transient Stability Analysis," *IEEE Trans. Circuits Syst.*, vol. 34, no. 2, pp. 160–173, Feb. 1987.

[32] A. Fouad and V. Vital, *Power System Transient Stability Analysis Using The Energy Function Method*. New Jersey, Prentice-Hall, 1992.

[33] J. Thorp and S. Naqavi, "Load Flow Fractals," in *Proc. of the 28th IEEE Conference on Decision and Control*, vol. 2, Dec. 1989, pp. 1822–1827.

[34] J. Thorp, S. Naqavi, and N. Chiang, "More Load Flow Fractals," in *Proc. of the 29th IEEE Conference on Decision and Control*, vol. 6, Dec. 1990, pp. 3028–3030.

[35] H. Chiang, F. Wu, and P. Varaiya, "A BCU Method for Direct Analysis of Power System Transient Stability," *IEEE Trans. Power Syst.*, vol. 9, no. 3, pp. 1194–1208, Aug. 1994.

[36] R. Treinen, V. Vittal, and W. Kliemann, "An Improved Technique to Determine the Controlling Unstable Equilibrium Point in a Power System," *IEEE Trans. Circuits Syst. I, Fundam. Theory Appl.*, vol. 43, no. 4, pp. 313–323, Apr. 1996.

[37] L. Chen, Y. Min, F. Xu, and K. Wang, "A Continuation-Based Method to Compute the Relevant Unstable Equilibrium Points for Power System Transient Stability Analysis," *IEEE Trans. Power Syst.*, vol. 24, no. 1, pp. 165–172, Feb. 2009.

[38] J. Lee and H. Chiang, "Convergent Regions of the Newton Homotopy Method for Nonlinear Systems: Theory and Computational Applications," *IEEE Trans. Circuits Syst. I, Fundam. Theory Appl.*, vol. 48, no. 1, pp. 51–66, Jan. 2001.

[39] I. Nazareno, L. Alberto, and N. Bretas, "Problems in the Precise Determination of BCU's Controlling Unstable Equilibrium Points and PEBS's Exit Point Method in Real-Time Transient Stability Analysis," in *Proc. IEEE/PES Trans. and Dist. Conf. Expo.: Latin America*, Nov. 2004, pp. 475–480.

[40] A. Llamas, J. De La Ree Lopez, L. Mili, A. Phadke, and J. Thorp, "Clarifications of the BCU Method for Transient Stability Analysis," *IEEE Trans. Power Syst.*, vol. 10, no. 1, pp. 210–219, Feb. 1995.

[41] A. Xue, S. Mei, and B. Xie, "A Comprehensive Method to Compute the Controlling Unstable Equilibrium Point," in *Third International Conference on Electric Utility Deregulation and Restructuring and Power Technologies*, Apr. 2008, pp. 1115–1120.

[42] J. Lee, "An Optimization-driven Framework for the Computation of the Controlling UEP in Transient Stability Analysis," *IEEE Trans. Autom. Control*, vol. 49, no. 1, pp. 115–119, Jan. 2004.

[43] J. Mitra, M. Benidris, and N. Cai, "Use of Homotopy-based Approaches in Finding Controlling Unstable Equilibrium Points in Transient Stability Analysis," in *to appear in the 19th Power Systems Computation Conference*, Genoa, Italy, June 2016, pp. 1–7.

[44] J. Lee and H. Chiang, "A Singular Fixed-Point Homotopy Method to Locate the Closest Unstable Equilibrium Point for Transient Stability Region Estimate," *IEEE Trans. Circuits Syst. II, Exp. Briefs*, vol. 51, no. 4, pp. 185–189, Apr. 2004.

[45] J. Lee, "A Novel Homotopy-based Algorithm for the Closest Unstable Equilibrium Point Method in Nonlinear Stability Analysis," in *Proc. of the International Symp. on Circuits and Syst.*, vol. 3, May 2003, pp. III–8–III–11.

[46] K. A. Nigim, S. Suryanarayanan, R. Gorur, and R. G. Farmer, "The Application of Analytical Hierarchy Process to Analyze the Impact of Hidden Failures in Special Protection Schemes," *Electric Power System Research*, vol. 67, no. 3, pp. 191–196, Dec. 2003.

[47] A. Fouad and V. Vittal, *Power System Transient Stability Analysis Using the Transient Energy Function Method*. Englewood Cliffs, NJ: Prentice-Hall, 1991.

[48] H. Chiu, "Sensitivity analysis of the transient energy function method," Ph.D. dissertation, Iowa State University, 1989.

[49] A. Wood and B. Wollenberg, *Power generation operation and control*. John Wiley and Sons, 1984.

[50] A. Fouad and T. Jianzhong, "Stability Constrained Optimal Rescheduling of Generation," *IEEE Trans. Power Syst.*, vol. 8, no. 1, pp. 105–112, Feb. 1993.

[51] openPDC. [Online]. Available: http://openpdc.codeplex.com/

[52] P. Yang, Z. Tan, A. Wiesel, and A. Nehora, "Power system state estimation using pmus with imperfect synchronization," *Power Systems, IEEE Transactions on*, vol. 28, no. 4, pp. 4162–4172, Nov 2013.

[53] M. Gol and A. Abur, "A fast decoupled state estimator for systems measured by pmus," 2014.

[54] B. Gou, "Generalized integer linear programming formulation for optimal pmu placement," *Power Systems, IEEE Transactions on*, vol. 23, no. 3, pp. 1099–1104, Aug 2008.

[55] S. Chakrabarti and E. Kyriakides, "Optimal placement of phasor measurement units for power system observability," *IEEE Transactions on Power Systems*, vol. 23, no. 3, pp. 1433–1440, Aug 2008.

[56] M. B. Mohammadi, R. A. Hooshmand, and F. H. Fesharaki, "A new approach for optimal placement of pmus and their required communication infrastructure in order to minimize the cost of the wams," *IEEE Transactions on Smart Grid*, vol. 7, no. 1, pp. 84–93, Jan 2016.

[57] A. Abur and A. G. Exposito, *Power System State Estimation: Theory And Implementation*. CRC Press, 2004.

[58] A. Monticelli, *State Estimation in Electric Power Systems: A Generalized Approach*. Springer Science & Business Media, 1999, vol. 507.

[59] J. Zhang, G. Welch, G. Bishop, and Z. Huang, "A two-stage Kalman filter approach for robust and real-time power system state estimation," *Sustainable Energy, IEEE Transactions on*, vol. 5, no. 2, pp. 629–636, April 2014.

[60] K. Fall and W. Stevens, *TCP/IP illustrated, volume 1: The protocols*. addison-Wesley, 2011.

[61] Microsoft. Windows Sockets 2. [Online]. Available: https://msdn.microsoft.com/en-us/library/windows/desktop/ms740673(v=vs.85).aspx